NASA TM X-547

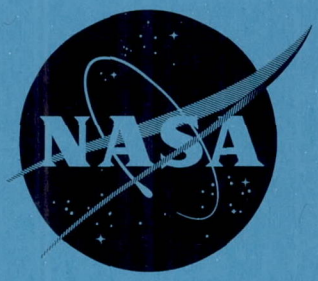

TECHNICAL MEMORANDUM

X-547

WIND-TUNNEL INVESTIGATION AT MACH NUMBERS FROM 0.30 TO 1.14 OF THE STATIC AERODYNAMIC CHARACTERISTICS OF MODIFIED MERCURY ESCAPE AND EXIT CAPSULE CONFIGURATIONS

By Albin O. Pearson

Langley Research Center
Langley Field, Va.

NATIONAL AERONAUTICS AND SPACE ADMINISTRATION
WASHINGTON
June 1961

NATIONAL AERONAUTICS AND SPACE ADMINISTRATION

TECHNICAL MEMORANDUM X-547

WIND-TUNNEL INVESTIGATION AT MACH NUMBERS FROM 0.30 TO 1.14 OF THE STATIC AERODYNAMIC CHARACTERISTICS OF MODIFIED MERCURY ESCAPE AND EXIT CAPSULE CONFIGURATIONS*

By Albin O. Pearson

SUMMARY

The pitching-moment, normal-force, and axial-force characteristics of a Mercury capsule with various modifications were investigated in the Langley 8-foot transonic pressure tunnel. The modifications consisted of adding a destabilizer flap to the exit configuration, increasing the diameter of the parachute housing of the exit and escape configurations, and adding a Marman clamp, tangential igniter cable fairings, and junction boxes to the escape configuration. The investigation was conducted for an angle-of-attack range which at a maximum varied from about -6° to 84° at Mach numbers from 0.30 to 1.14. The Reynolds number varied from about 1.3×10^6 to 3.7×10^6.

The results of the investigation show that for the escape configuration a slight reduction in the static longitudinal stability occurred with the addition of the tangential igniter cable fairings and junction boxes but that the addition of the Marman clamp, in combination with the other modifications, produced a substantial increase in the stability. For the exit configuration the addition of the modifications tended to destabilize the model only at Mach numbers less than about 0.90 at low angles of attack.

INTRODUCTION

The static aerodynamic characteristics of a nonlifting reentry capsule for use in Project Mercury are given in references 1 and 2 for transonic and supersonic speeds, respectively. For these investigations the data for

*Title, Unclassified.

the escape configuration (capsule with escape tower and rocket attached) are limited to angles of attack less than about 21°.

Since the publication of references 1 and 2, however, several modifications to the Mercury configurations have been made. These modifications consist of adding a destabilizer flap to the exit model, increasing the diameter of the parachute housing of the exit, escape, and reentry configurations, and adding a Marman clamp, tangential igniter cable fairings, and junction boxes to the escape configuration. The use of a canted face on the escape rocket to increase the miss distance between the escape configuration and main booster rocket after separation of the capsule from the booster has also been proposed. Additional wind-tunnel tests have, therefore, been made by the National Aeronautics and Space Administration to determine the static aerodynamic characteristics of models having these modifications and also to extend the angle-of-attack range of the escape configuration at transonic speeds. Results obtained from tests at supersonic and hypersonic speeds of modified exit and escape configurations are given in reference 3.

The present investigation was performed in the 8-foot transonic pressure tunnel and provides static aerodynamic data at subsonic and transonic speeds for models of the escape configuration with and without modifications at angles of attack to a maximum of approximately 84°. In addition, a model of the exit configuration with the increased parachute-housing diameter and destabilizer flap was tested at angles of attack to near 84°. The investigation was conducted at Mach numbers from 0.30 to 1.14 and at Reynolds numbers which varied from about 1.3×10^6 to 3.7×10^6.

SYMBOLS

The data presented herein are referred to the body system of axes with the origin located at the model center-of-gravity position. The positive directions of forces, moments, and displacements are shown in figure 1. The coefficients and symbols are defined as follows:

A	maximum body cross-sectional area, sq ft
C_A	axial-force coefficient, $\frac{\text{Axial force}}{qA}$
$C_{A,\alpha \approx 0}$	axial-force coefficient at $\alpha \approx 0°$
C_m	pitching-moment coefficient, $\frac{\text{Pitching moment}}{qAd}$

C_{m_α} slope of pitching-moment coefficient at $\alpha \approx 0^\circ$, $\frac{\partial C_m}{\partial \alpha}$, per degree

C_N normal-force coefficient, $\frac{\text{Normal force}}{qA}$

C_{N_α} slope of normal-force coefficient at $\alpha \approx 0^\circ$, $\frac{\partial C_N}{\partial \alpha}$, per degree

$C_{p,c}$ model-balance chamber-pressure coefficient, $\frac{\text{Model chamber pressure - Free-stream static pressure}}{q}$

d maximum body diameter, in.

M free-stream Mach number

q free-stream dynamic pressure, lb/sq ft

r radius, in.

R Reynolds number based on maximum body diameter and free-stream conditions

α angle of attack of model center line, deg

MODELS, TESTS, AND ACCURACY

Details of the models tested are shown in figure 2 and photographs are presented in figure 3. The capsule portion of all models consisted of a hollow body of revolution made from aluminum alloy. For the escape configuration a cylindrical aluminum-alloy body, simulating a rocket container, was mounted on a tower made from three cross-braced steel rods attached to the smaller end of the conical capsule. The three tower rods formed an equilateral triangle, and the escape-configuration models were oriented in the tunnel so that the base of this triangle was in a horizontal plane when the model angle of attack was 0°.

A 1/7-scale model of the escape configuration was tested to determine the effects of the Marman clamp at angles of attack to a maximum of about 14°. One-ninth-scale models of both the exit and escape configurations were used for the remainder of the investigation. The models were mounted on a three-component, internally located, strain-gage balance and were sting supported. Several model sting-support arrangements were used in order to maintain the models near the tunnel center line throughout the angle-of-attack range (fig. 3) and also to attempt to minimize the effects of sting interference.

The tests were conducted in the Langley 8-foot transonic pressure tunnel at a dewpoint such that the airflow was free of condensation shocks. For most of the investigation the stagnation pressure was maintained at about 1.0 atmosphere. For the tests of the escape configuration at angles of attack greater than 40°, however, it was necessary to reduce the stagnation pressure to as low as about 0.33 atmosphere due to load limits on the strain-gage balance. The variation of Reynolds number, based on model maximum diameter and free-stream conditions, with Mach number is shown in figure 4 for the various models tested.

Normal force, axial force, and pitching moment were determined with the pitching moments referred to the center of gravity of the various models as shown in figure 2. The axial-force results are gross values and have not been adjusted to a condition of free-stream static pressure at the base. The model-balance chamber-pressure coefficient $C_{p,c}$ was determined from the model-chamber pressure measured by means of an orifice located inside the model in the strain-gage-balance chamber.

Based upon balance accuracy (neglecting any sting interference effects), it is estimated that the coefficients of normal force, axial force, and pitching moment are accurate within ±0.075, ±0.075, and ±0.020, respectively, at a Mach number of 0.30, but at a Mach number of 1.14 and a stagnation pressure of 1.0 atmosphere the coefficients are accurate within ±0.011, ±0.011, and ±0.003, respectively. The maximum variation of the actual test Mach numbers from the presented nominal values is less than ±0.005. All data presented from this investigation are essentially free of wall-reflected disturbances. Corrections were applied for tunnel-flow angularity and for model sting and balance deflections. The accuracy of the angle of attack is estimated to be within ±0.20°.

RESULTS AND DISCUSSION

It is shown in reference 1, for models and sting-support systems similar to those of the present investigation, that some interference effects due to sting-support arrangements are indicated at the higher angles of attack. These effects, for a 1/7-scale model, are negligible on the pitching-moment and axial-force characteristics and on the normal-force coefficients are a maximum of about 4 percent of the presented faired values. Although the models used for the higher angles of attack of the present investigation are smaller (1/9 scale) than those of reference 1, the interference effects are probably essentially the same in magnitude.

The pitching-moment, normal-force, and axial-force characteristics of the various configurations investigated are presented in figures 5

to 8 and are summarized in figure 9. The variations of model-chamber-pressure coefficient with angle of attack are shown in figure 10.

Escape Configuration

Aerodynamic force and moment characteristics are presented in figure 5 and summarized in figure 9(a) for the escape configuration with and without tangential igniter cable fairings and junction boxes attached to the escape rocket. A slight reduction in the slope of the pitching-moment curve is indicated near an angle of attack of 0° when the igniter cable fairings and junction boxes are attached and the trim points at Mach numbers less than 1.03 are shifted less than 2°. The addition of the igniter cable fairings and junction boxes also tended to increase the normal-force coefficients at Mach numbers less than 1.03 (fig. 5(b)) but had essentially no effect on the slope of the normal-force curve (fig. 9(a)). The axial-force coefficients (fig. 5(c)) were essentially unaffected.

The addition of the Marman clamp resulted in a substantial increase in the static stability of the model near an angle of attack of 0° (figs. 6(a) and 9(b)) along with an increase in the magnitude of the normal-force coefficients and the slope of the normal-force curve (figs. 6(b) and 9(b)); however, this effect of the Marman clamp on C_N and C_{N_α} tended to diminish as the Mach number was increased. The magnitudes of the axial-force coefficients were only slightly reduced near an angle of attack of 0° (figs. 6(c) and 9(b)), but some increase was indicated at the higher angles of attack.

The aerodynamic force and moment characteristics of the model with the igniter cable fairings, junction boxes, increased parachute housing, and Marman clamp are shown in figure 7 and summarized in figure 9(c). A comparison of these data with those of figures 5 and 9(a) for the model without modifications (ref. 1) indicates that at the lower angles of attack the combined effects of the modifications substantially increased the stability of the model and increased the normal-force coefficients and slope of the normal-force curve; these changes are primarily due to the addition of the Marman clamp.

The data of figure 7 also indicate that canting the face of the escape rocket 10° from the vertical can provide small changes in trim angle of attack but has little or no effect on the slope of the pitching-moment curve or on the normal-force or axial-force characteristics.

Exit Configuration

Results from the tests of the modified exit configuration show that the combined effects of the destabilizer flap and increased parachute housing tended to destabilize the configuration only at the lower Mach numbers and angles of attack with essentially no effect at Mach numbers above 0.90. (See fig. 9(d).) It is interesting to note that although the flap did not have a large destabilizing influence on the model stability, it did reduce the unstable trim angle of attack near 0° by as much as 5°. (See fig. 8(a).)

Addition of the modifications to the model increased the magnitude of the normal-force coefficients at angles of attack up to about 28° (fig. 8(b)) for the lower Mach numbers, but at a Mach number of 1.14 the increase in normal-force coefficient extended to an angle of attack of approximately 54°. At intermediate angles of attack, from the above values to near 70°, there is a substantial reduction in the normal-force coefficients. The slope of the normal-force curve (fig. 9(d)) is increased up to Mach numbers near 1.00 with a maximum increase of about 25 percent occurring at a Mach number near 0.70.

The axial-force coefficients for the modified model are reduced at the higher angles of attack (fig. 8(c)), but essentially no effect of the modifications is shown in $C_{A,\alpha \approx 0}$ (fig. 9(d)).

CONCLUSIONS

The static aerodynamic characteristics of models of exit and escape configurations of a Mercury capsule modified to include a destabilizer flap and increased parachute-housing diameter on the exit configuration and tangential igniter cable fairings, junction boxes, a Marman clamp, and increased parachute-housing diameter on the escape configuration were investigated in the Langley 8-foot transonic tunnel from Mach numbers from a minimum of 0.30 to about 1.14. The results of the investigation indicate the following:

1. A slight reduction in the static longitudinal stability of the escape configuration occurs with the addition of the tangential igniter cable fairings and junction boxes, but the addition of the Marman clamp in combination with the other modifications produces a substantial increase in the stability.

2. The addition of the destabilizer flap and increased parachute-housing diameter to the exit configuration tend to destabilize the model only at Mach numbers less than about 0.90 and at low angles of attack.

Langley Research Center,
National Aeronautics and Space Administration,
Langley Field, Va., April 19, 1961.

REFERENCES

1. Pearson, Albin O.: Wind-Tunnel Investigation at Mach Numbers From 0.50 to 1.14 of the Static Aerodynamic Characteristics of a Model of a Project Mercury Capsule. NASA TM X-292, 1960.

2. Shaw, David S., and Turner, Kenneth L.: Wind-Tunnel Investigation of the Static Aerodynamic Characteristics of a 1/9-Scale Model of a Project Mercury Capsule at Mach Numbers From 1.60 to 4.65. NASA TM X-291, 1960.

3. Pearson, Albin O.: Wind-Tunnel Investigation at Mach Numbers From 3.0 to 6.8 of the Static Aerodynamic Characteristics of Modified Mercury Exit and Escape Capsule Configurations. NASA TM X-324, 1960.

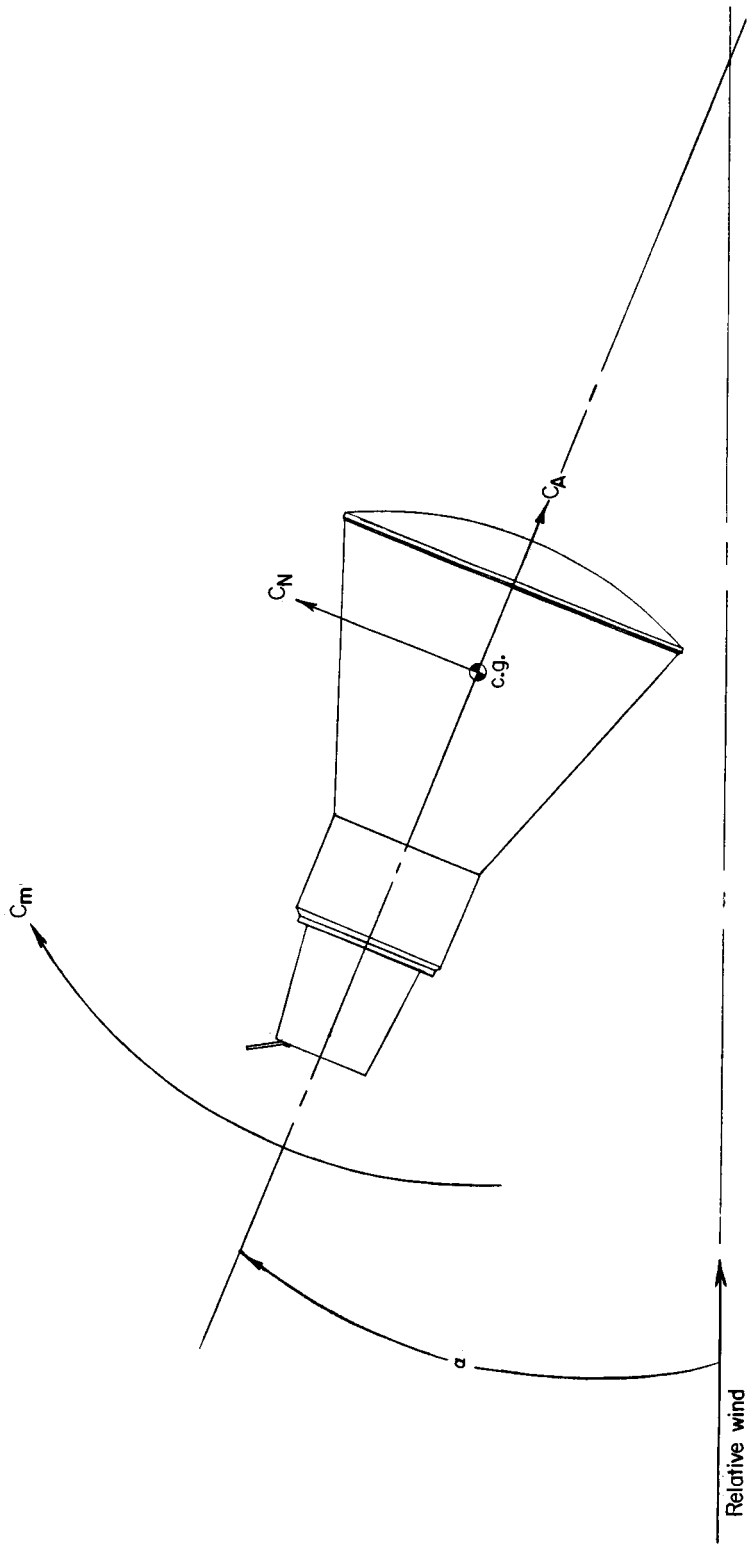

Figure 1.- Body axis system (exit configuration shown). Arrows indicate positive direction.

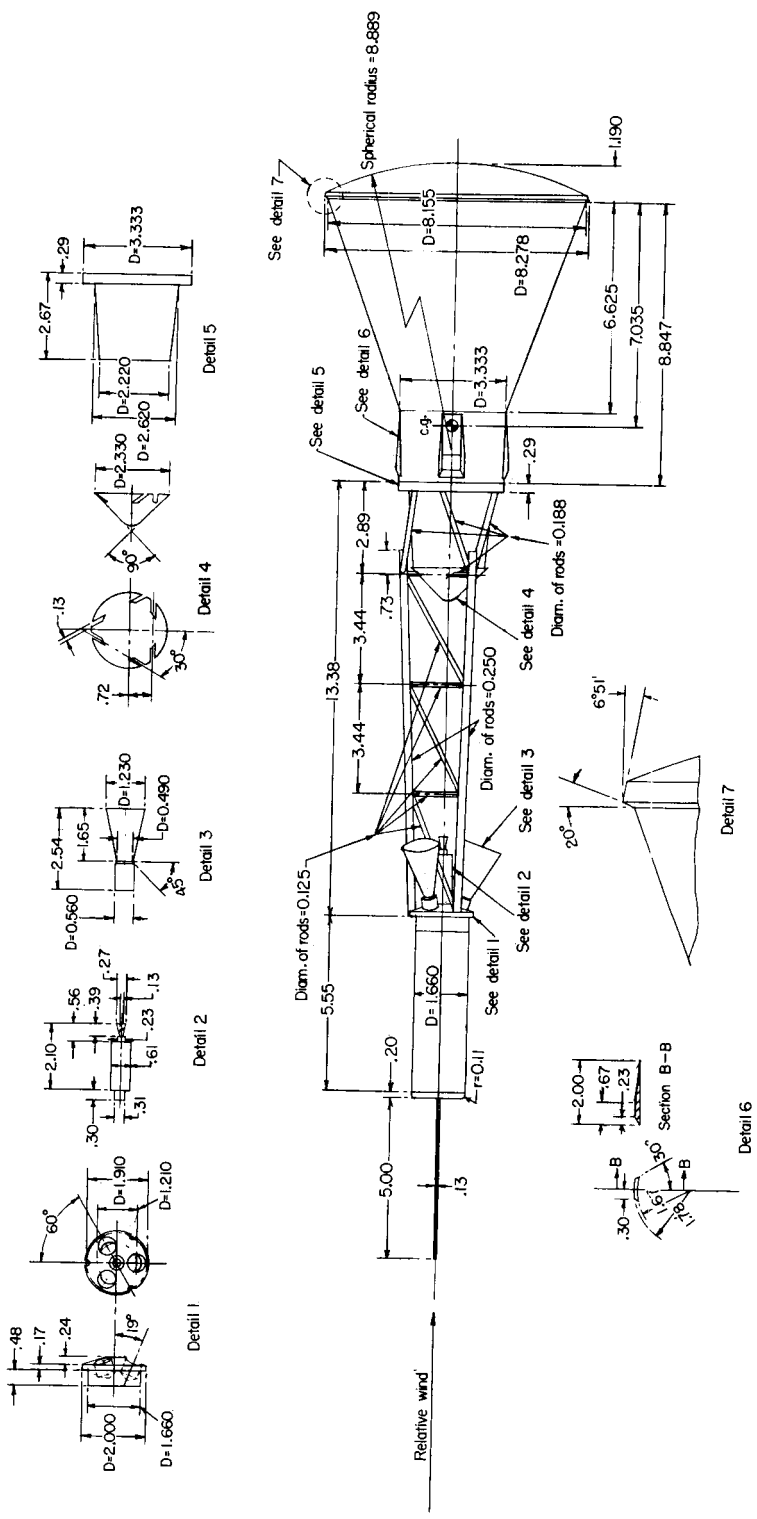

(a) Escape configuration with no modifications (1/9-scale model).

Figure 2.- Details of model configurations. All dimensions are in inches unless otherwise noted.

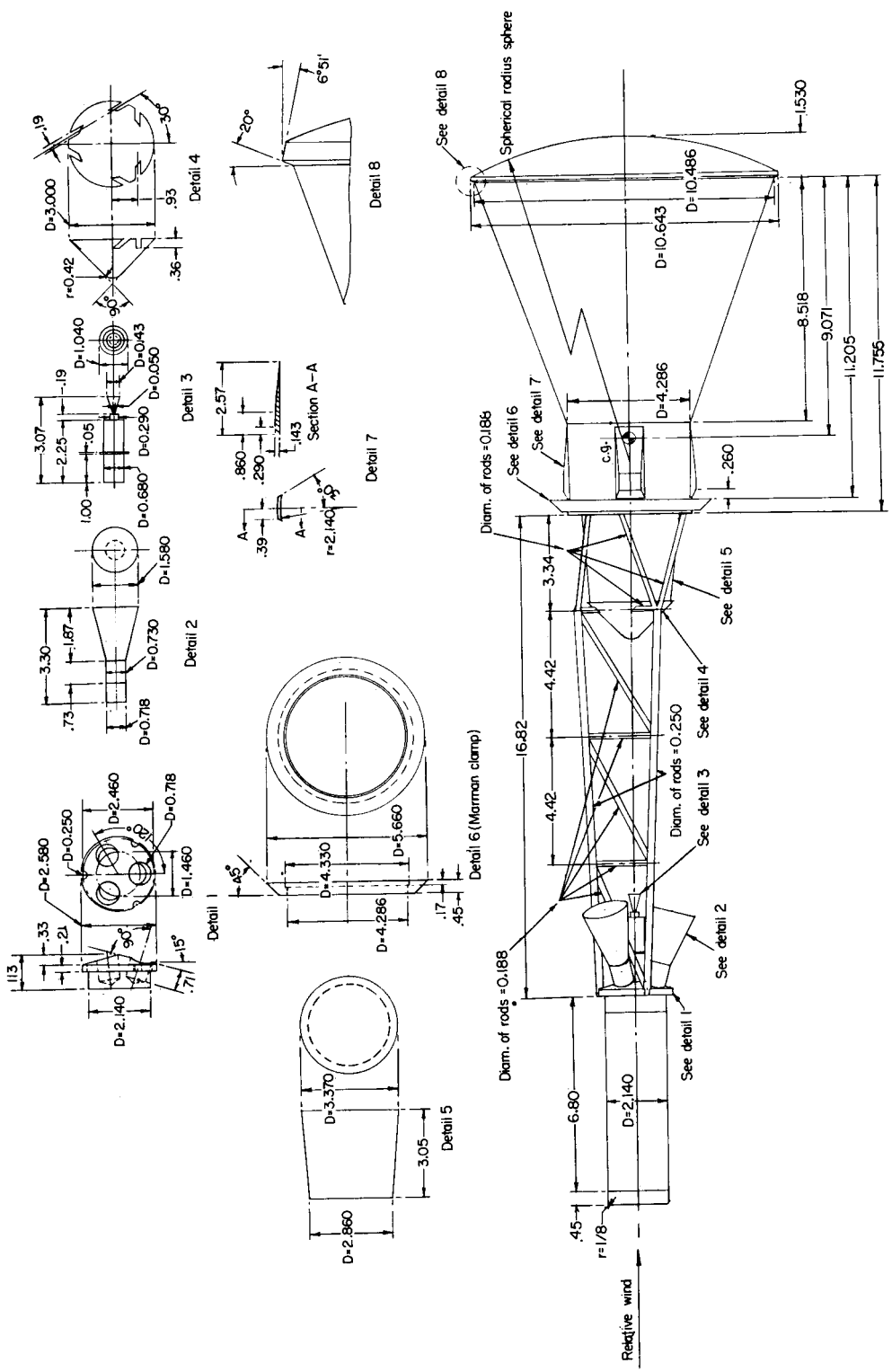

(b) Escape configuration with Marman clamp (1/7-scale model).

Figure 2.- Continued.

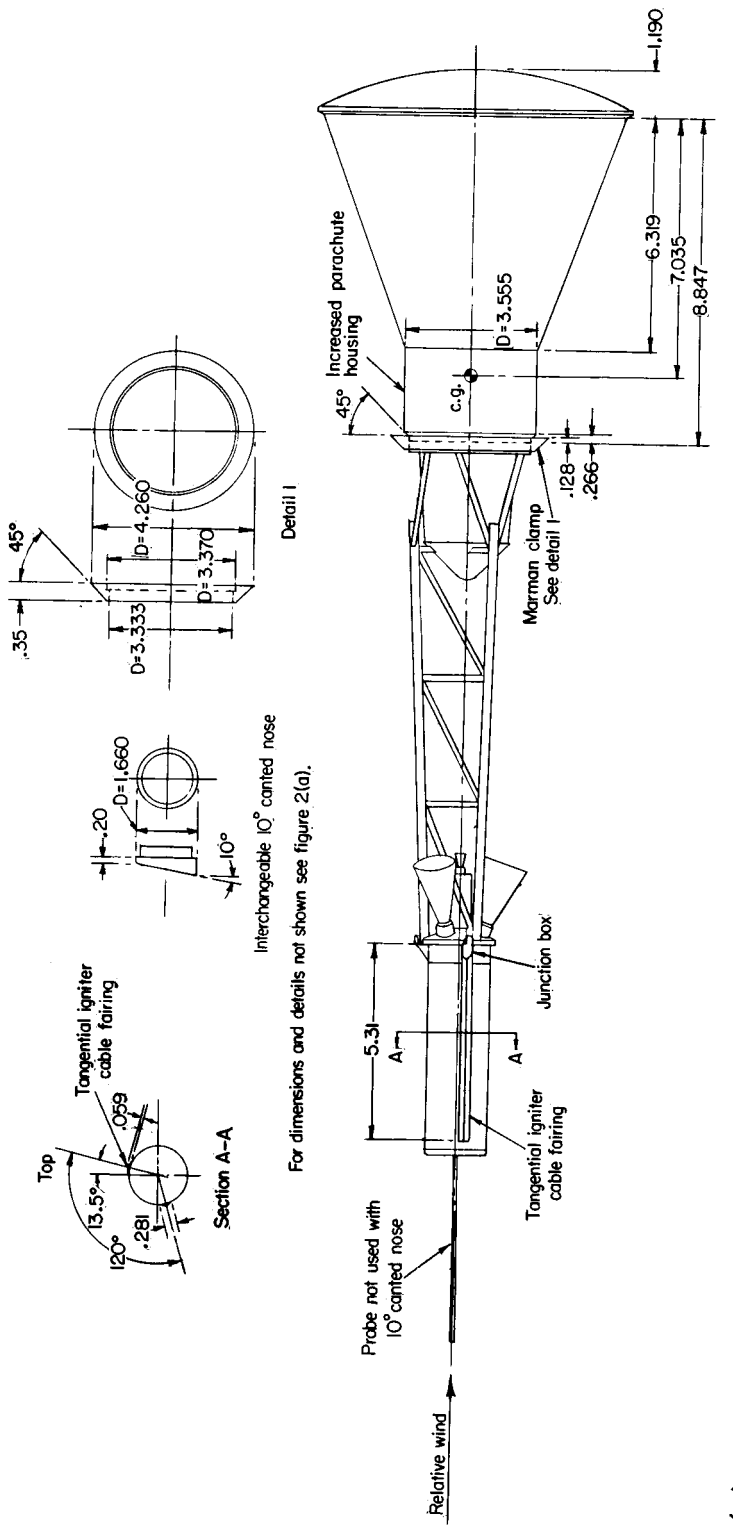

(c) Escape configuration with tangential igniter cable fairings, junction boxes, Marman clamp, and increased parachute-housing diameter (1/9-scale model).

Figure 2.- Continued.

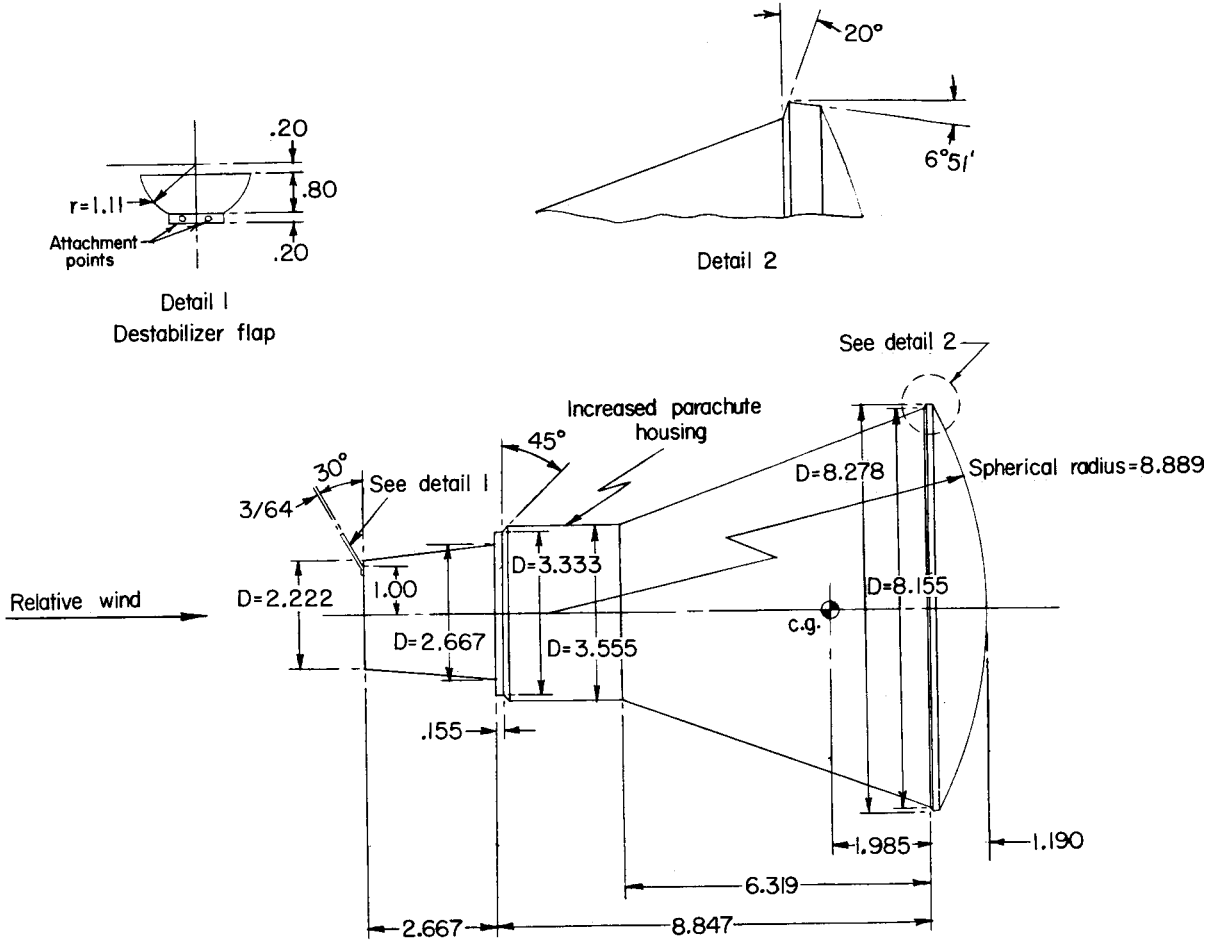

(d) Exit configuration with destabilizer flap and increased parachute-housing diameter (1/9-scale model).

Figure 2.- Concluded.

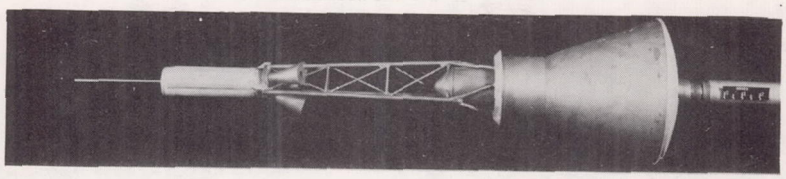

$\alpha \approx -6°$ to 19° L-60-4745

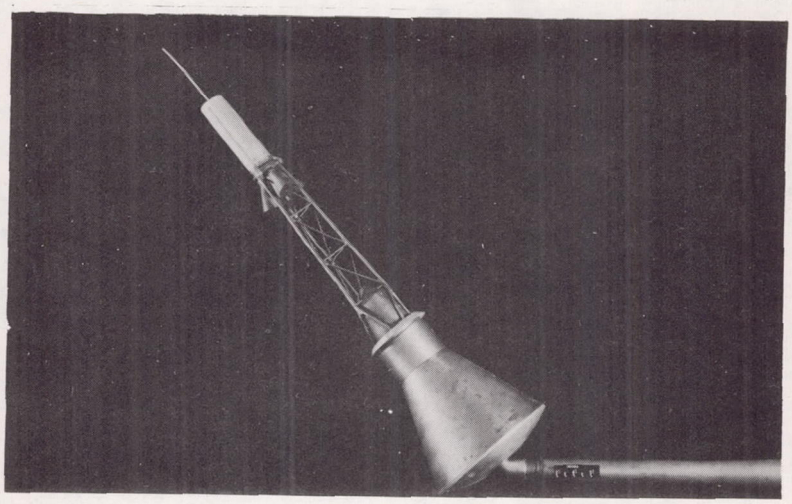

$\alpha \approx 30°$ to 52° L-60-4748

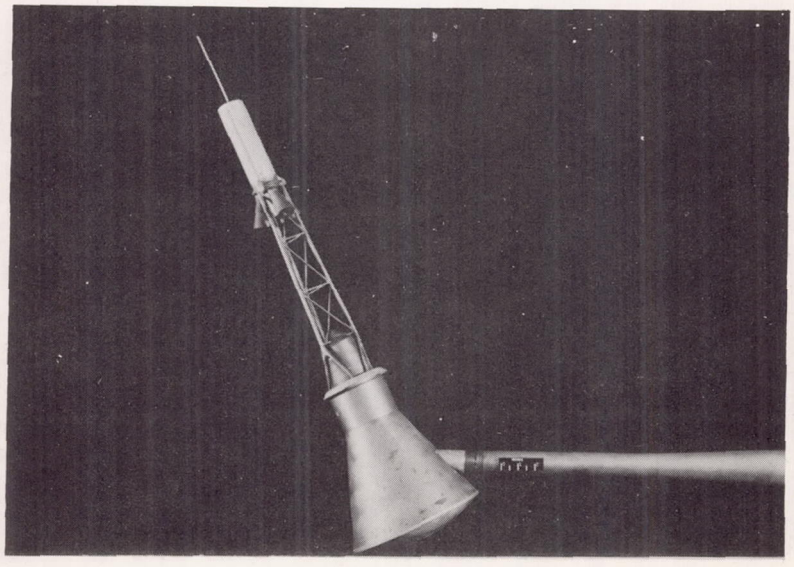

$\alpha \approx 60°$ to 84°

(a) Escape configuration. L-60-4749

Figure 3.- Model configurations and sting-support arrangements.

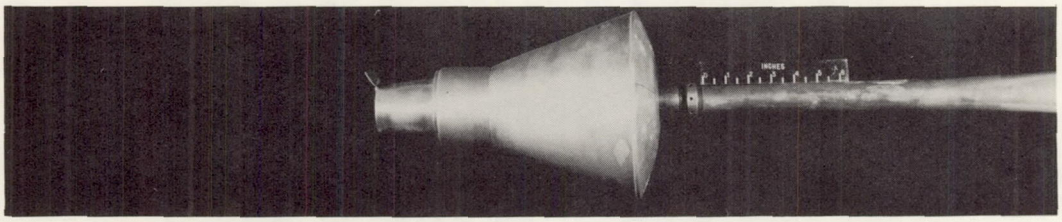

$\alpha \approx -6°$ to 19° L-60-2977

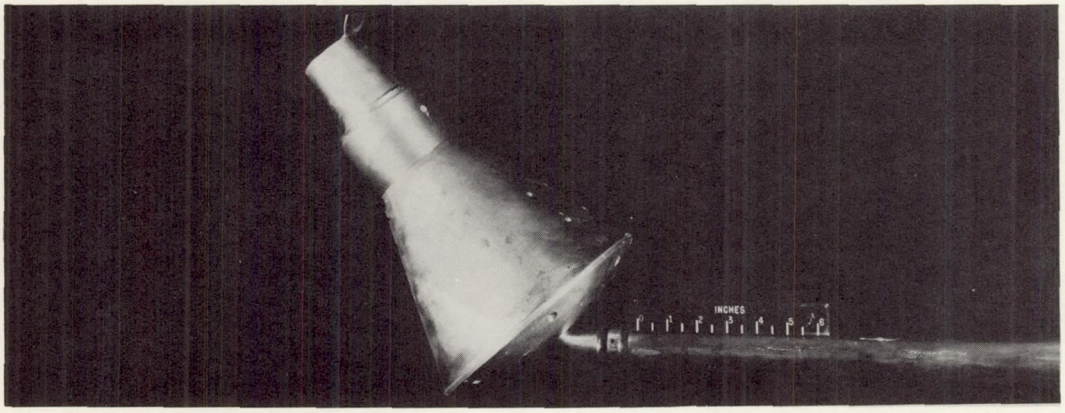

$\alpha \approx 30°$ to 52° L-60-2981

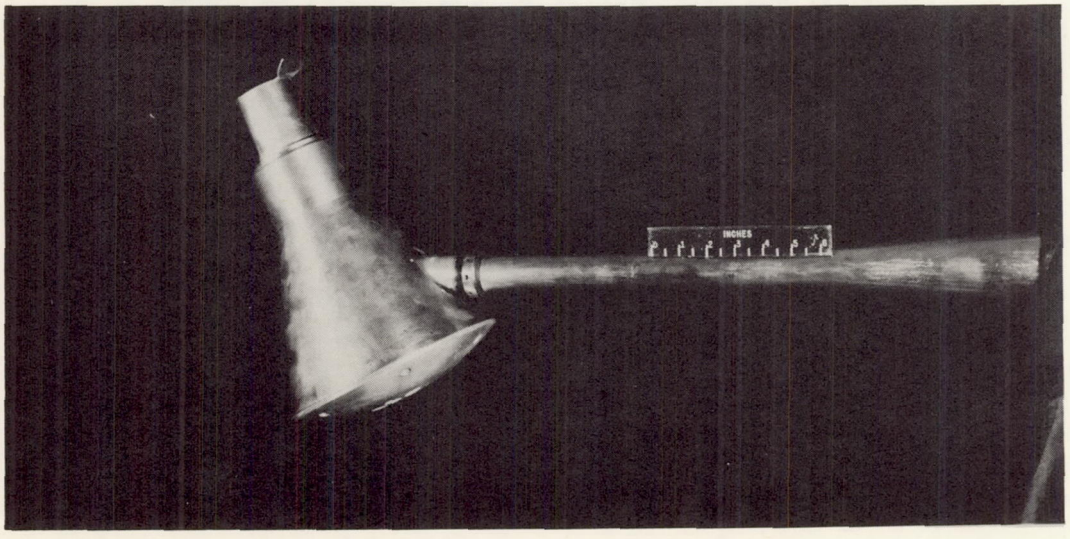

$\alpha \approx 60°$ to 84°

(b) Exit configuration. L-60-2980

Figure 3.- Concluded.

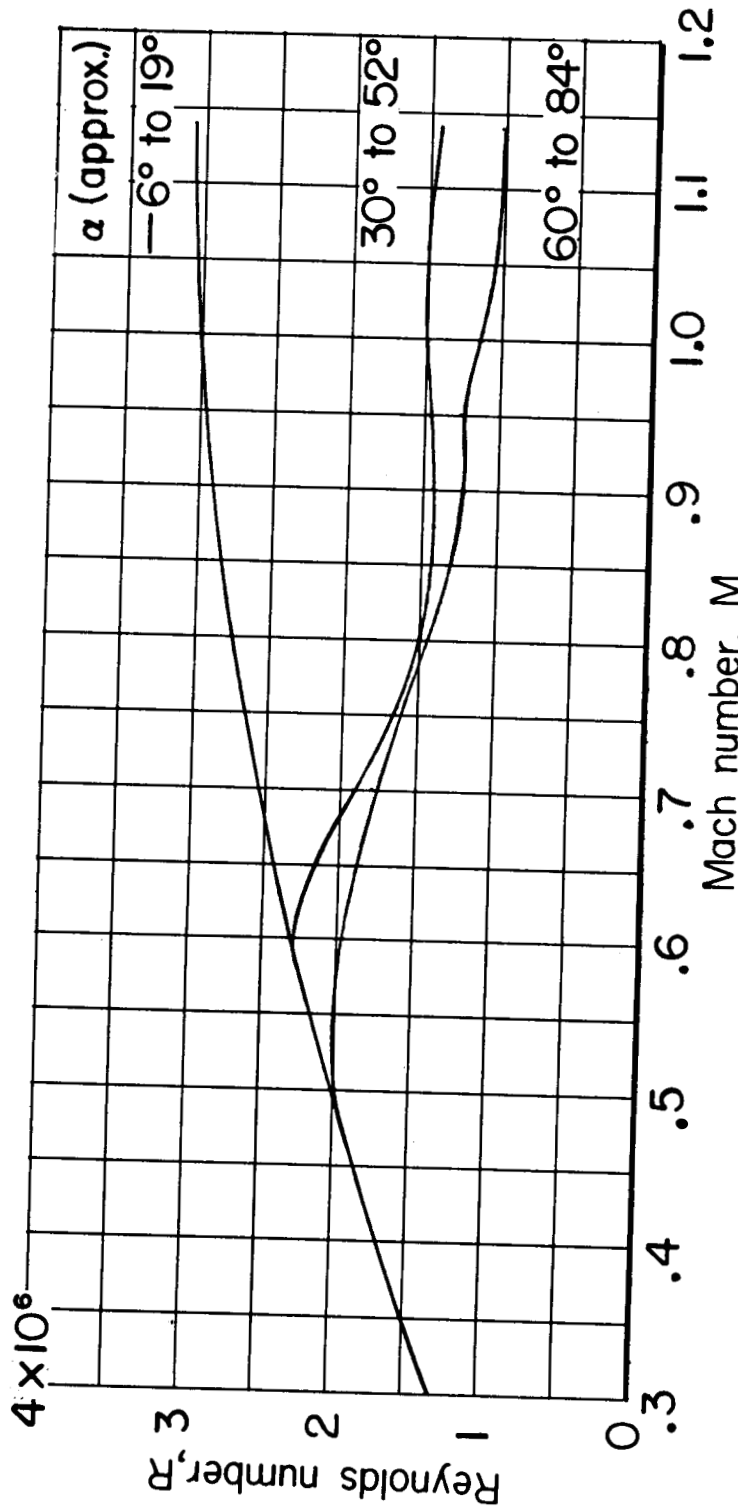

(a) 1/9-scale escape configuration.

Figure 4.- Variation of Reynolds number, based on maximum diameter and free-stream conditions, with Mach number.

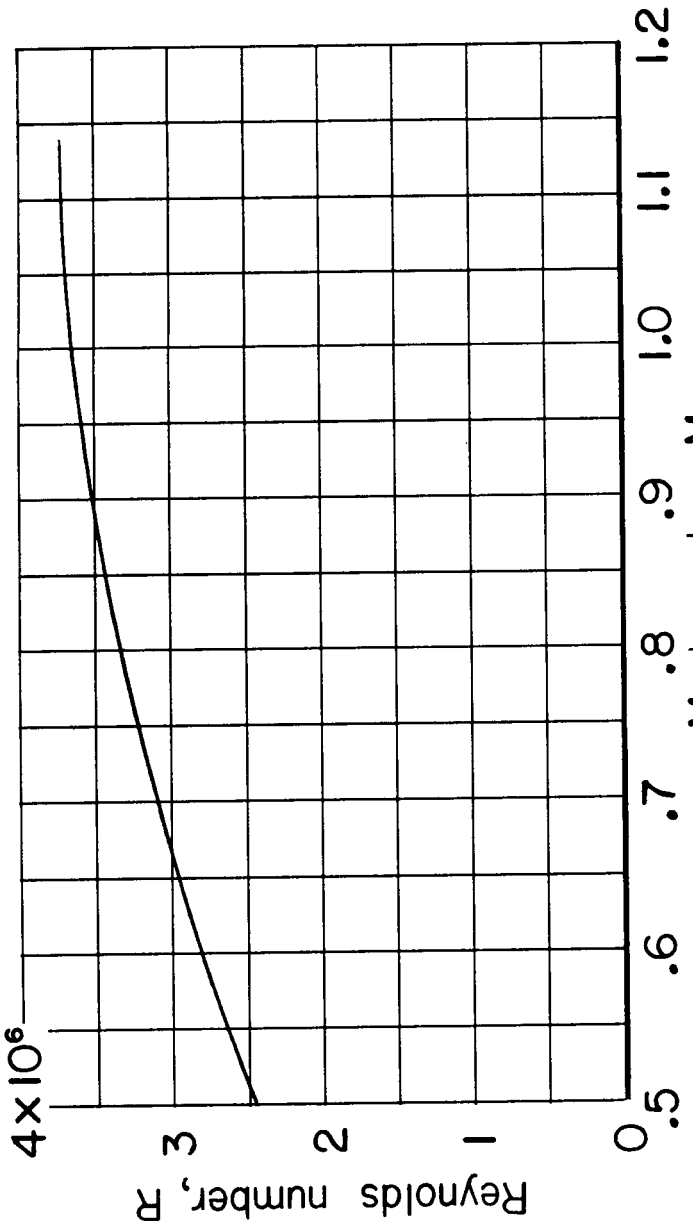

(b) 1/7-scale escape configuration.

Figure 4.- Continued.

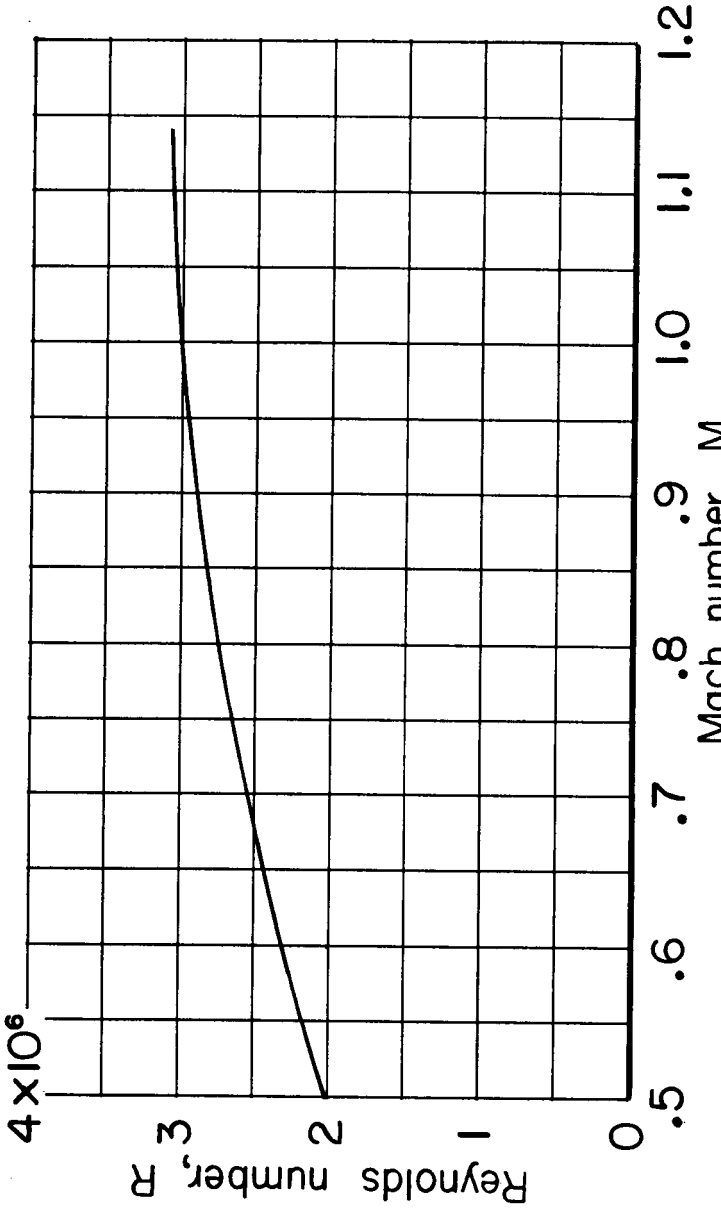

(c) 1/9-scale exit configuration.

Figure 4.- Concluded.

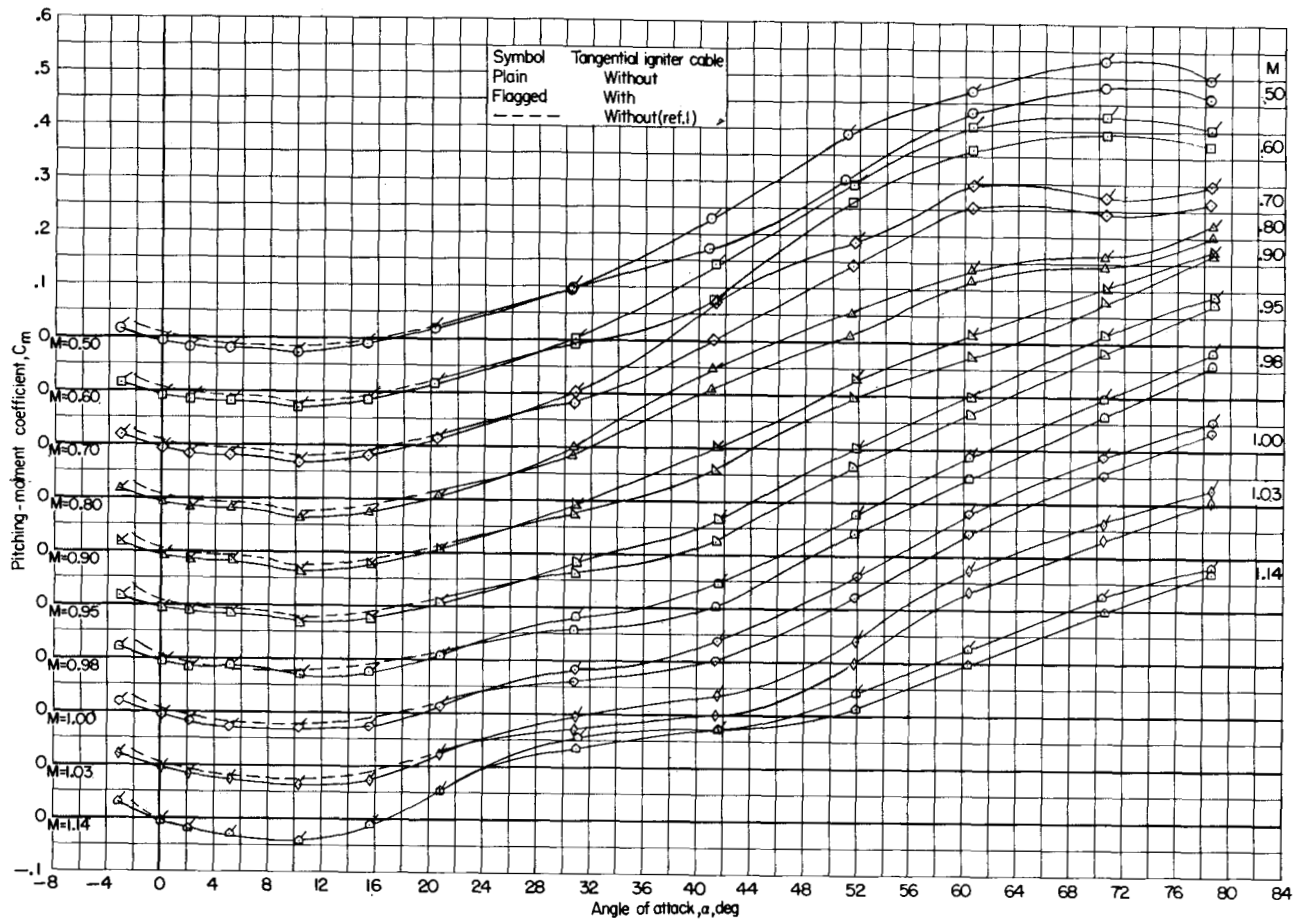

(a) Variation of C_m with α.

Figure 5.- Static aerodynamic characteristics of escape configuration in pitch (1/9-scale model with and without tangential igniter cable fairings and junction boxes).

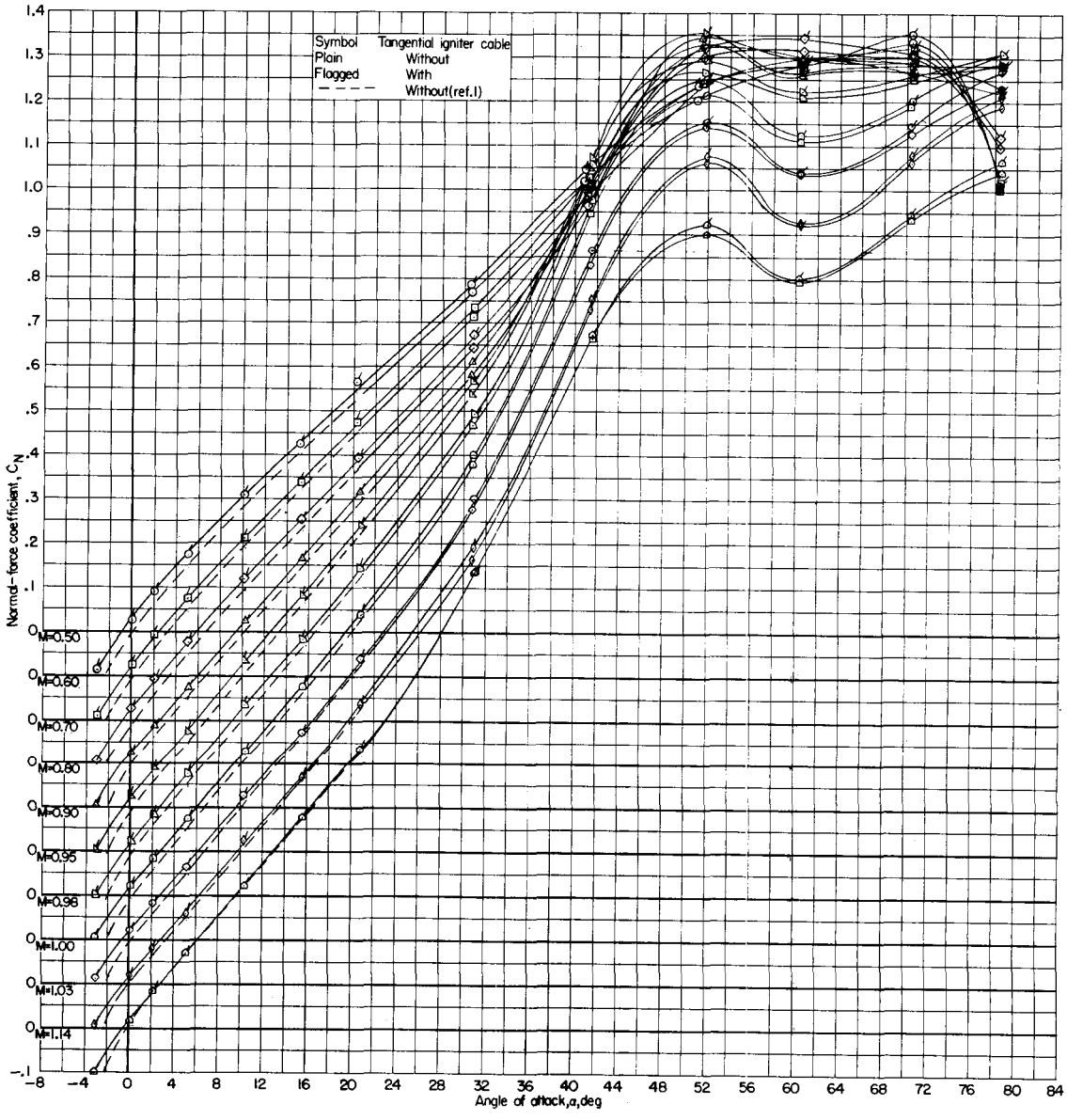

(b) Variation of C_N with α.

Figure 5.- Continued.

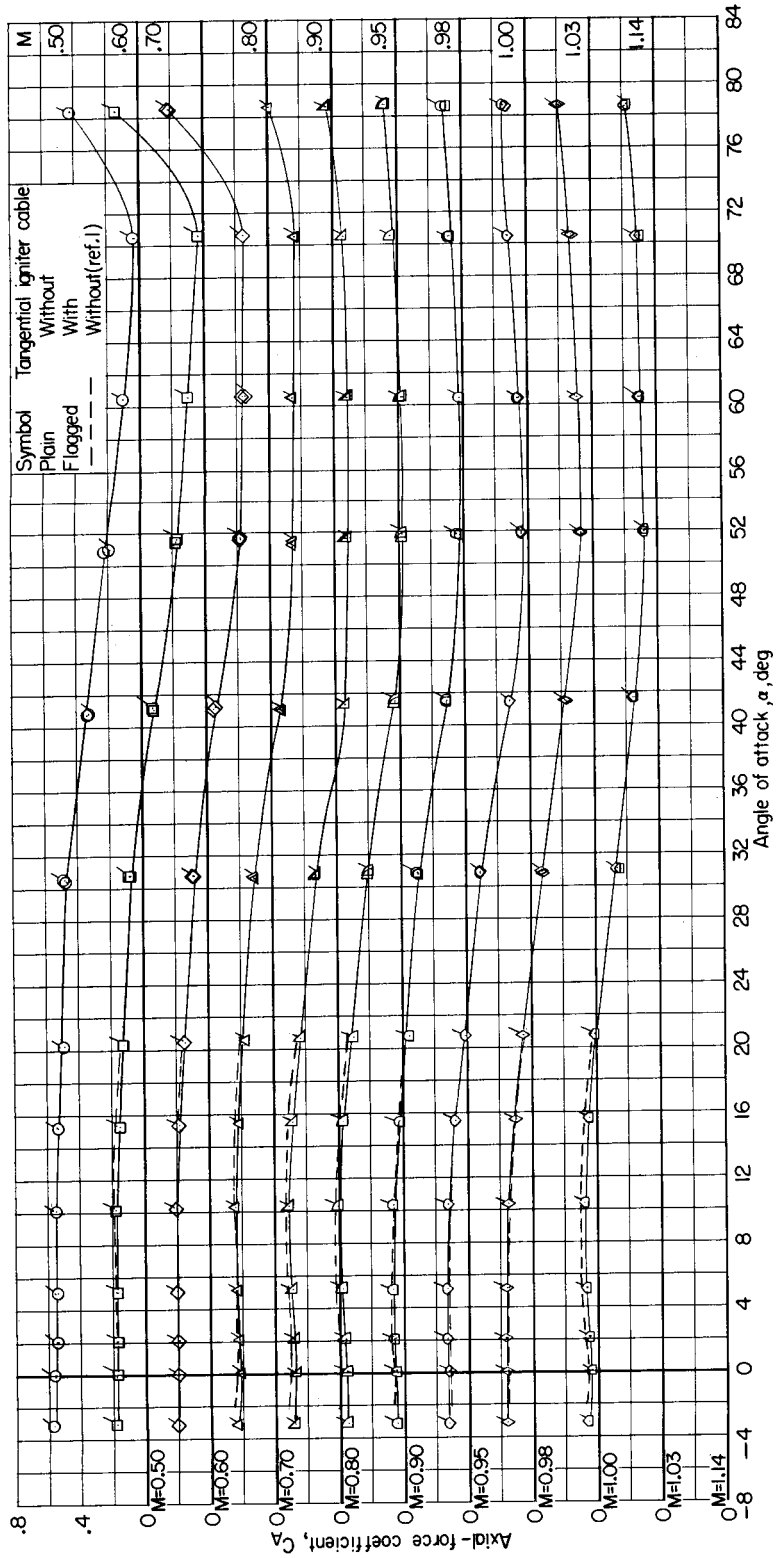

(c) Variation of C_A with α.

Figure 5.- Concluded.

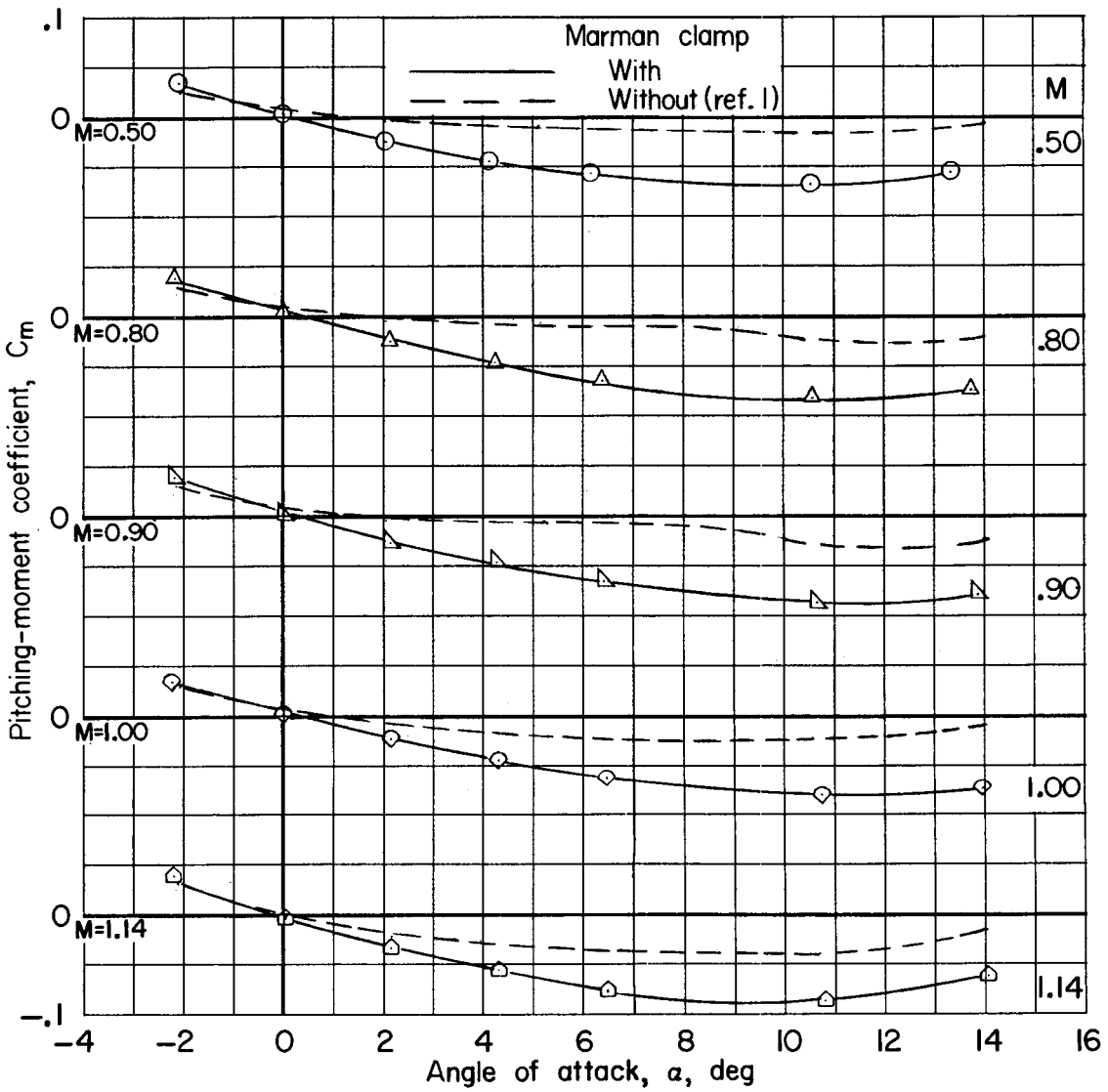

(a) Variation of C_m with α.

Figure 6.- Static aerodynamic characteristics of escape configuration in pitch (1/7-scale model with Marman clamp).

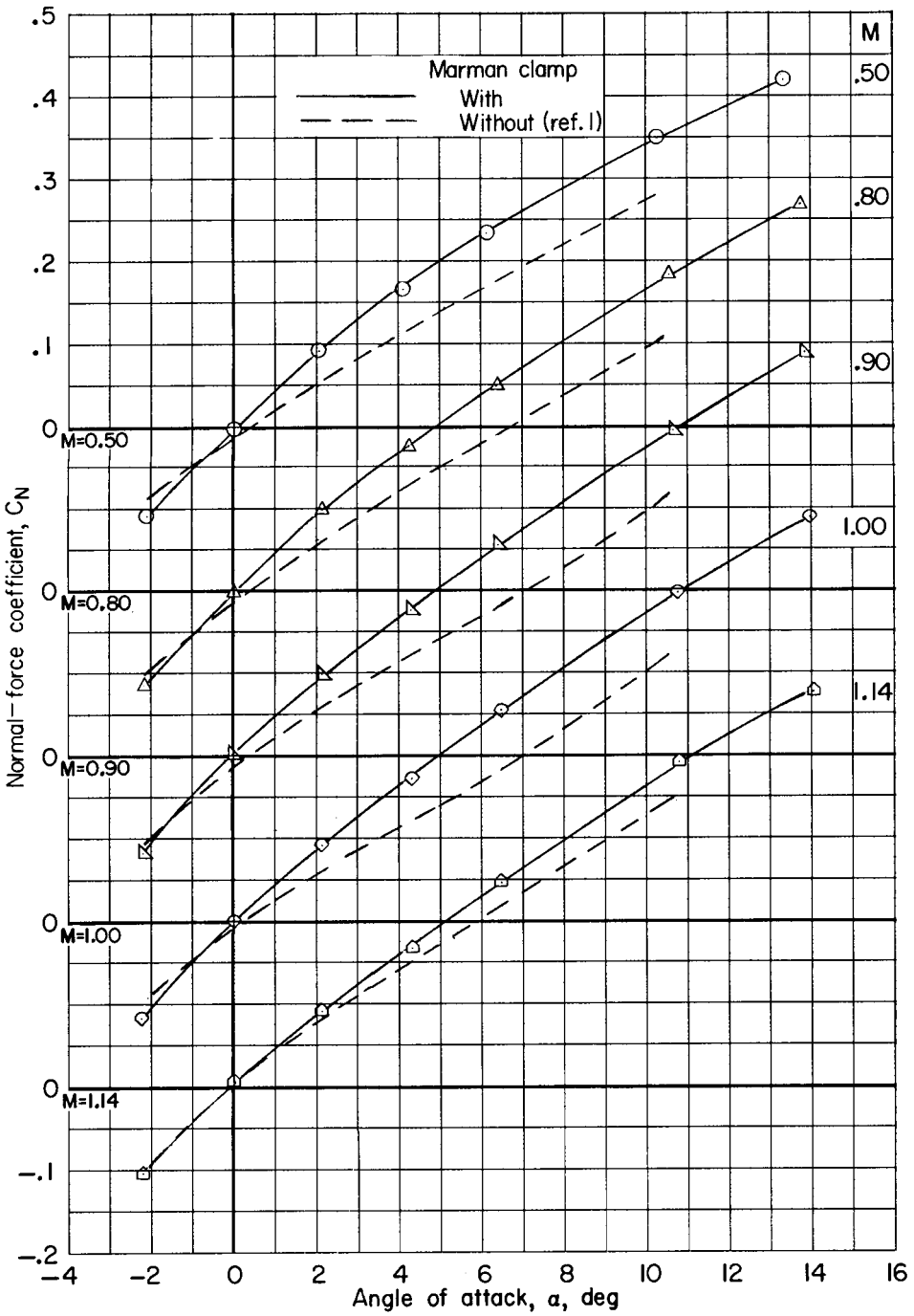

(b) Variation of C_N with α.

Figure 6.- Continued.

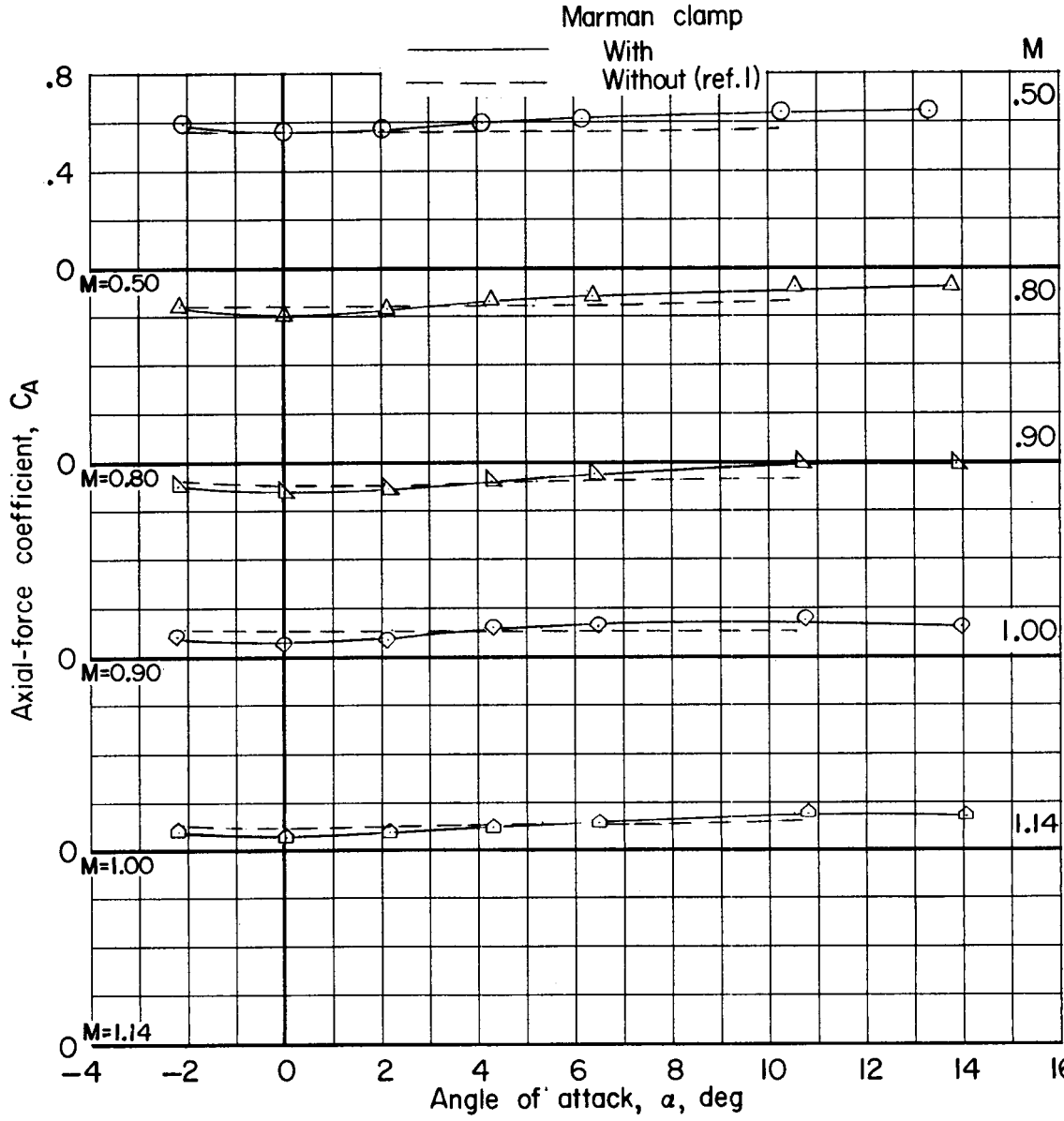

(c) Variation of C_A with α.

Figure 6.- Concluded.

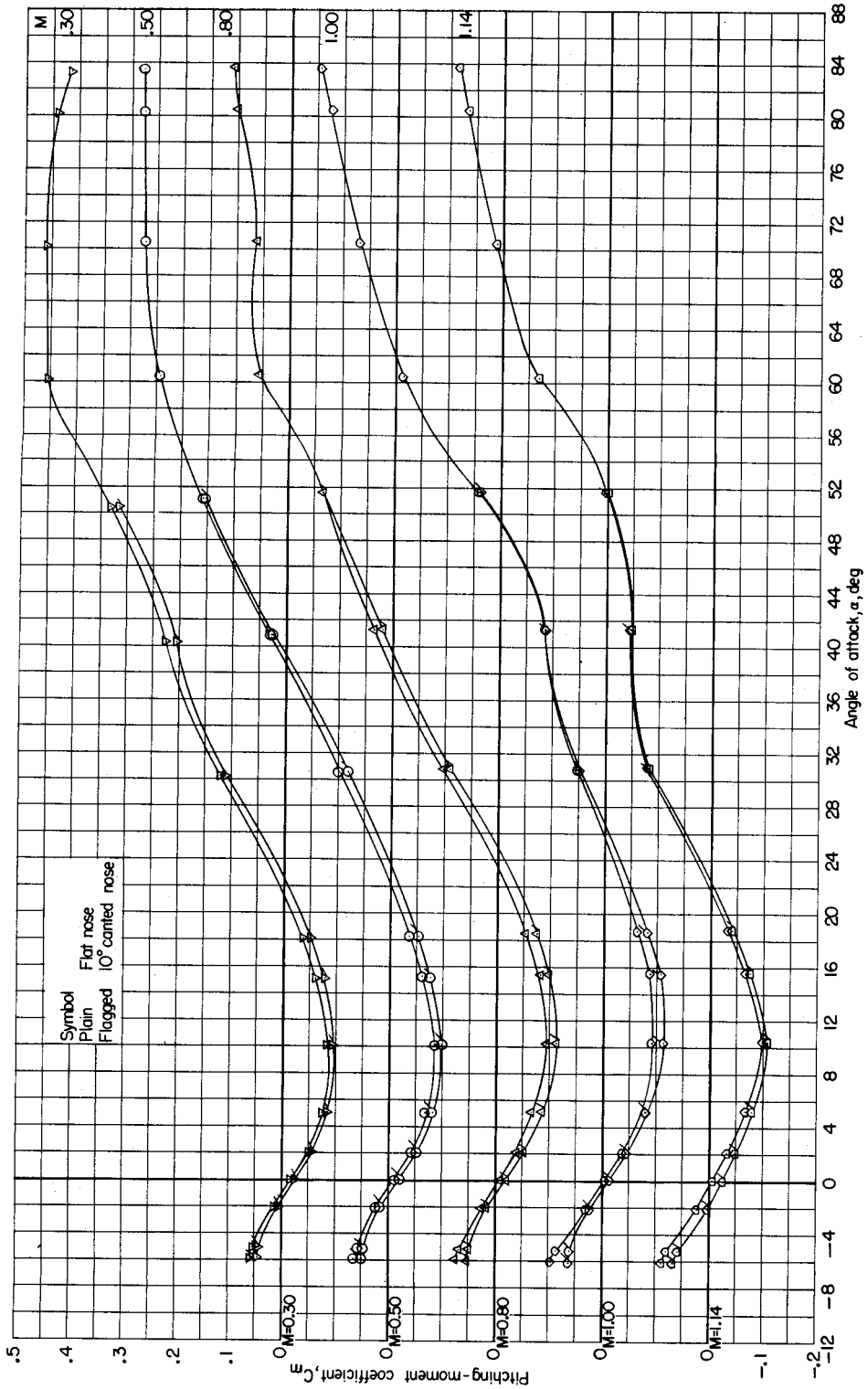

(a) Variation of C_m with α.

Figure 7.- Static aerodynamic characteristics of escape configuration in pitch with nose cants of 0° or 10° (1/9-scale model with tangential igniter cable fairings, junction boxes, Marman clamp, and increased parachute housing diameter).

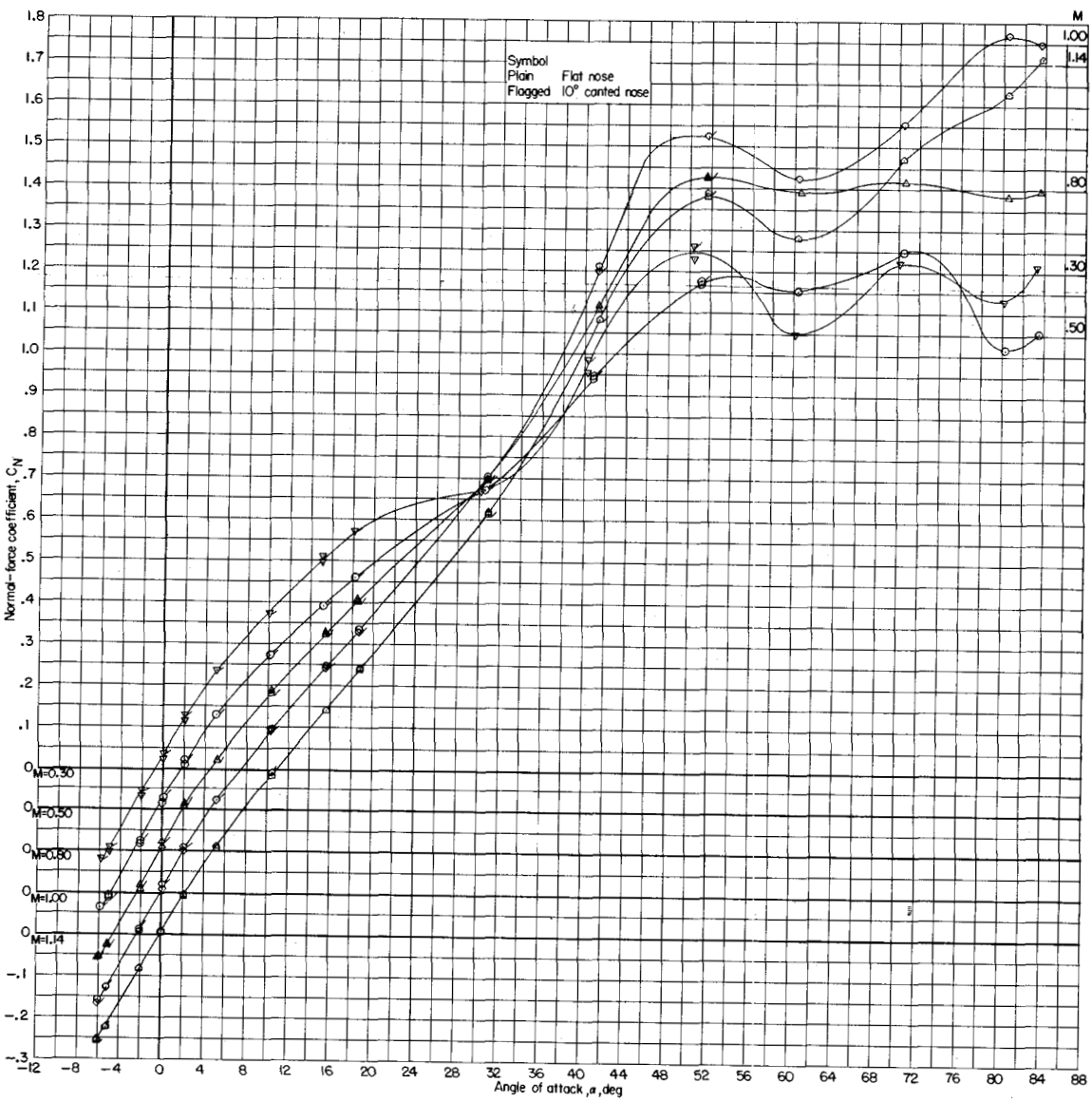

(b) Variation of C_N with α.

Figure 7.- Continued.

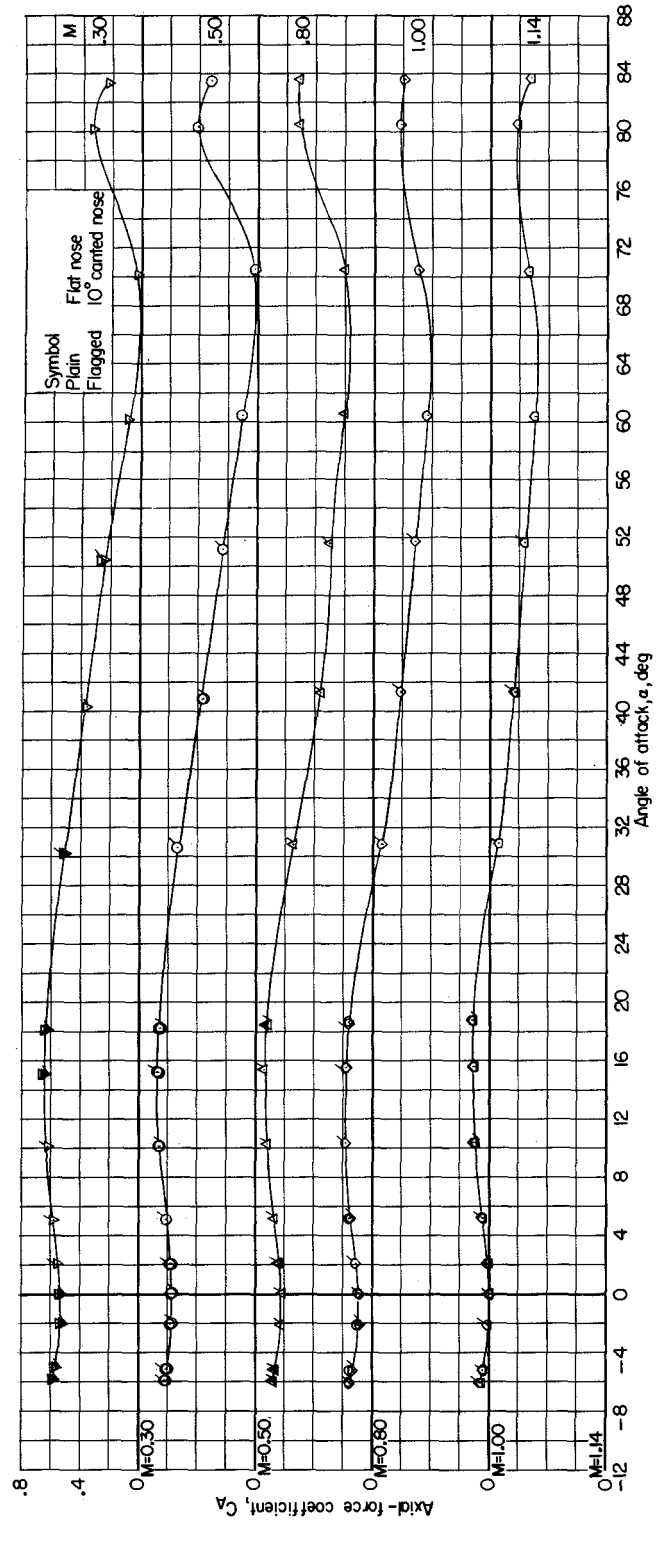

(c) Variation of C_A with α.

Figure 7.- Concluded.

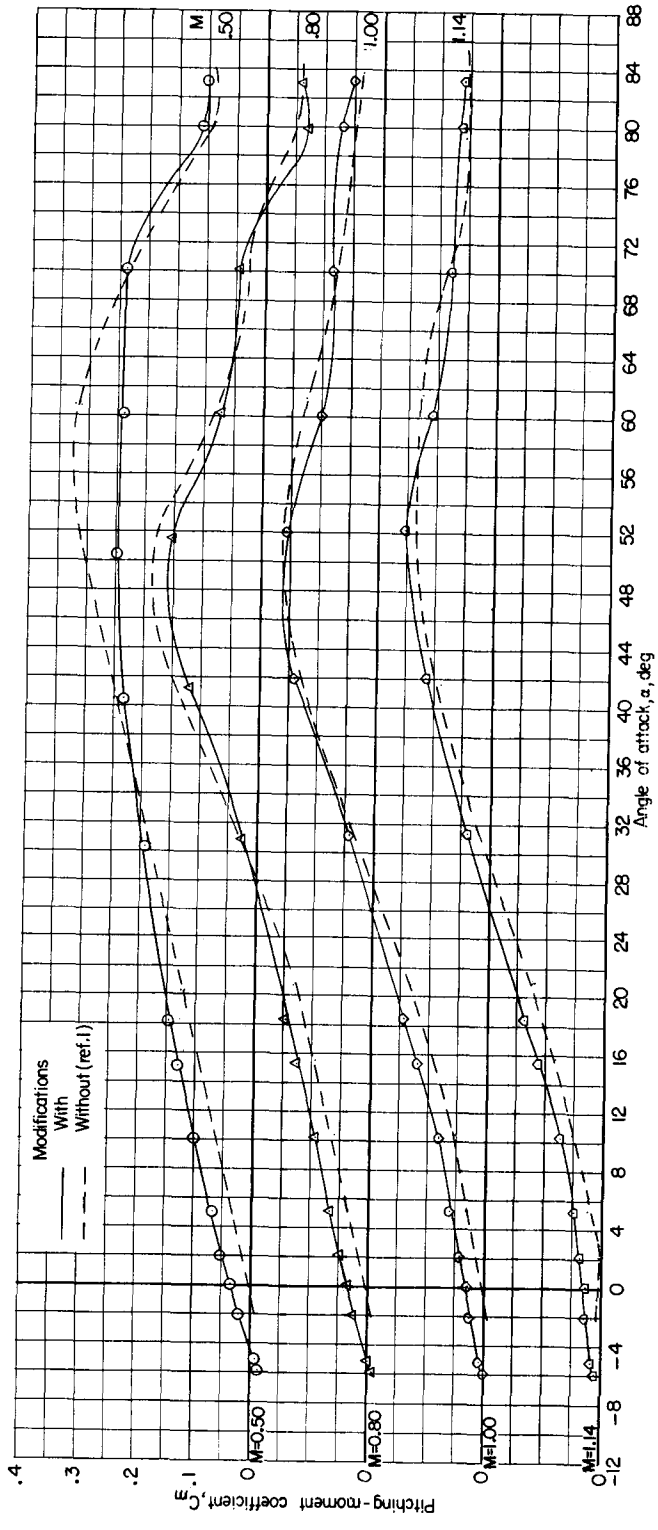

(a) Variation of C_m with α.

Figure 8.- Static aerodynamic characteristics of exit configuration in pitch (1/9-scale model with destabilizer flap and increased parachute housing).

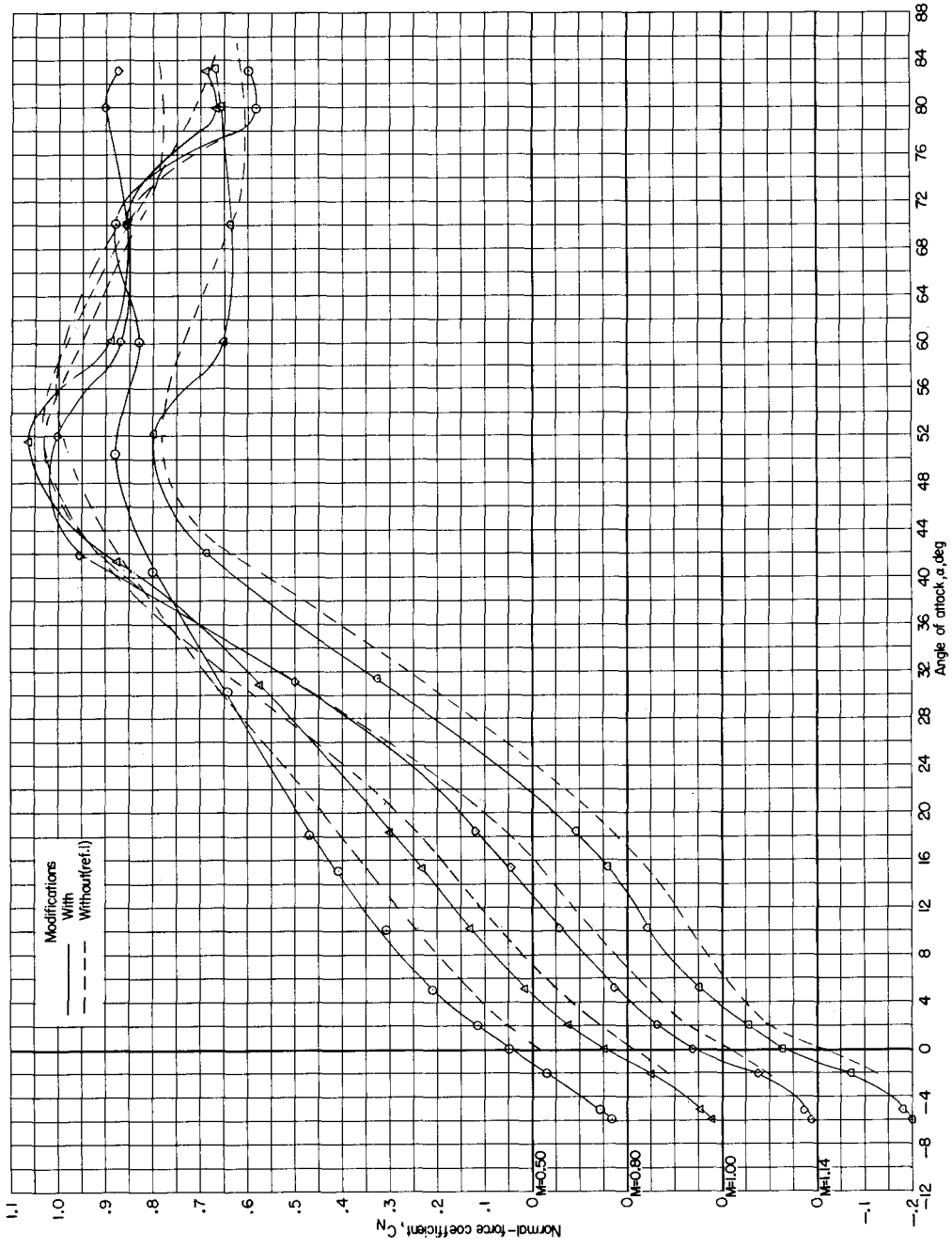

(b) Variation of CN with α.

Figure 8.- Continued.

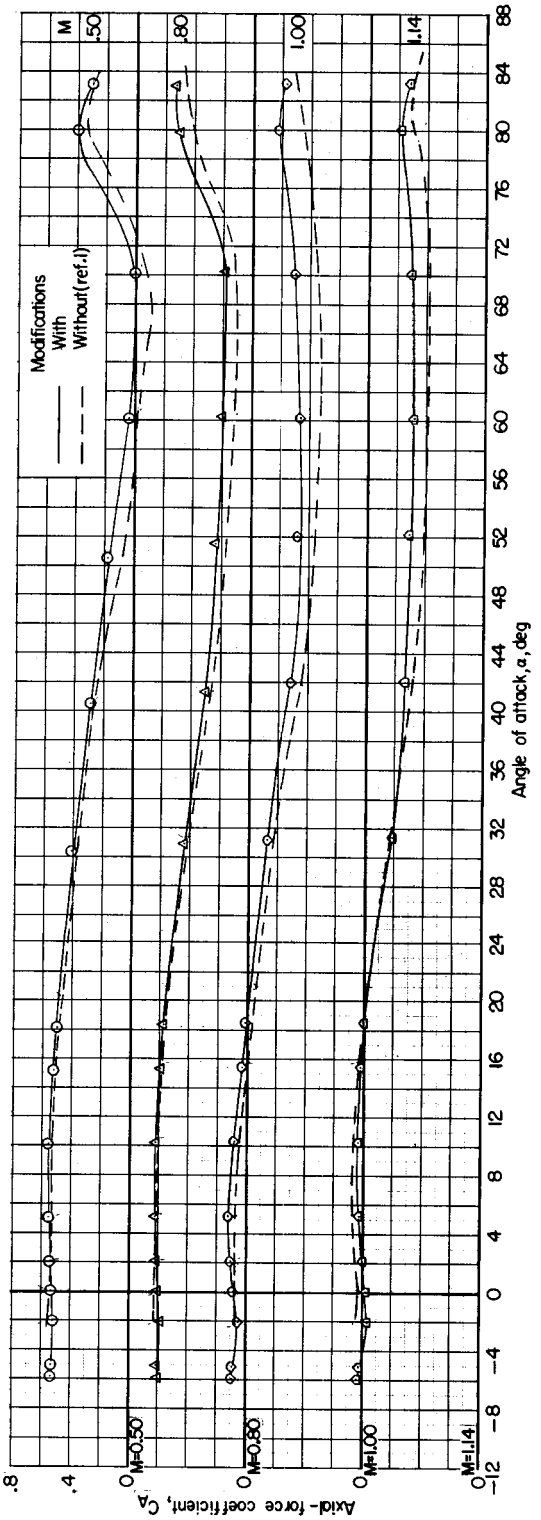

(c) Variation of C_A with α.

Figure 8.- Concluded.

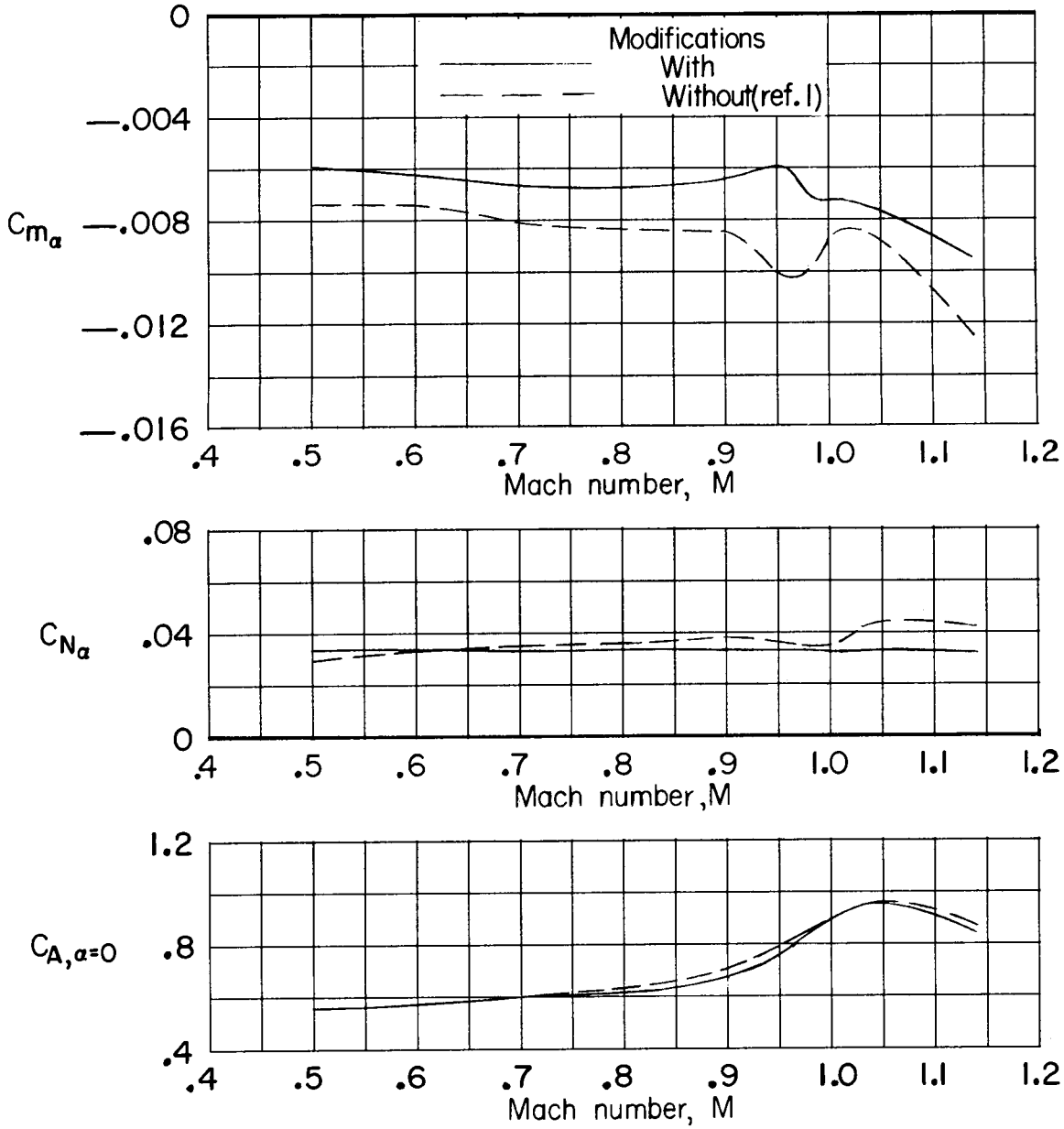

(a) Escape configuration with and without tangential igniter cable fairings and junction boxes.

Figure 9.- Summary of static aerodynamic characteristics of models in pitch.

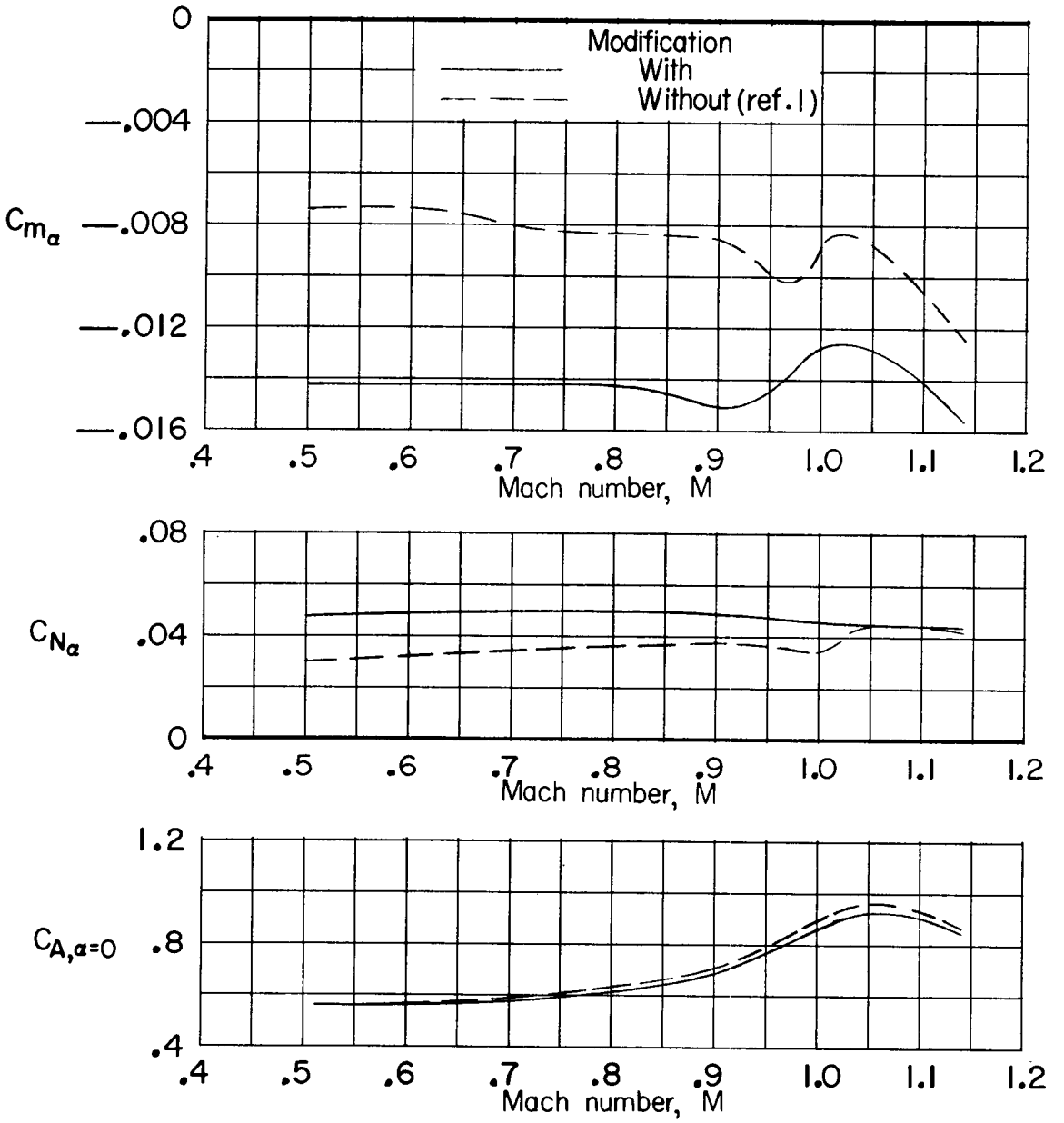

(b) Escape configuration with Marman clamp.

Figure 9.- Continued.

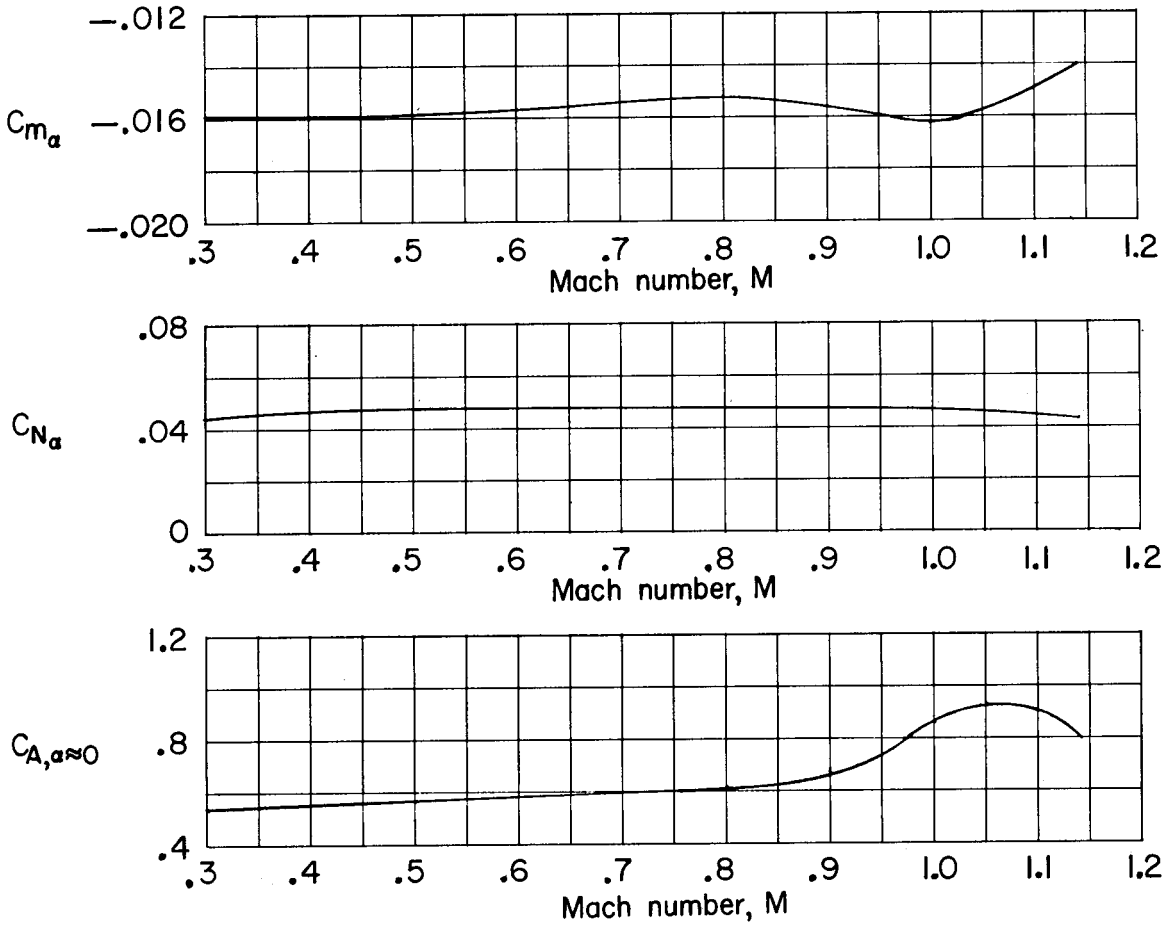

(c) Escape configuration with tangential igniter cable fairings, junction boxes, Marman clamp, and increased parachute-housing diameter. Data for nose cants of 0° or 10° are identical.

Figure 9.- Continued.

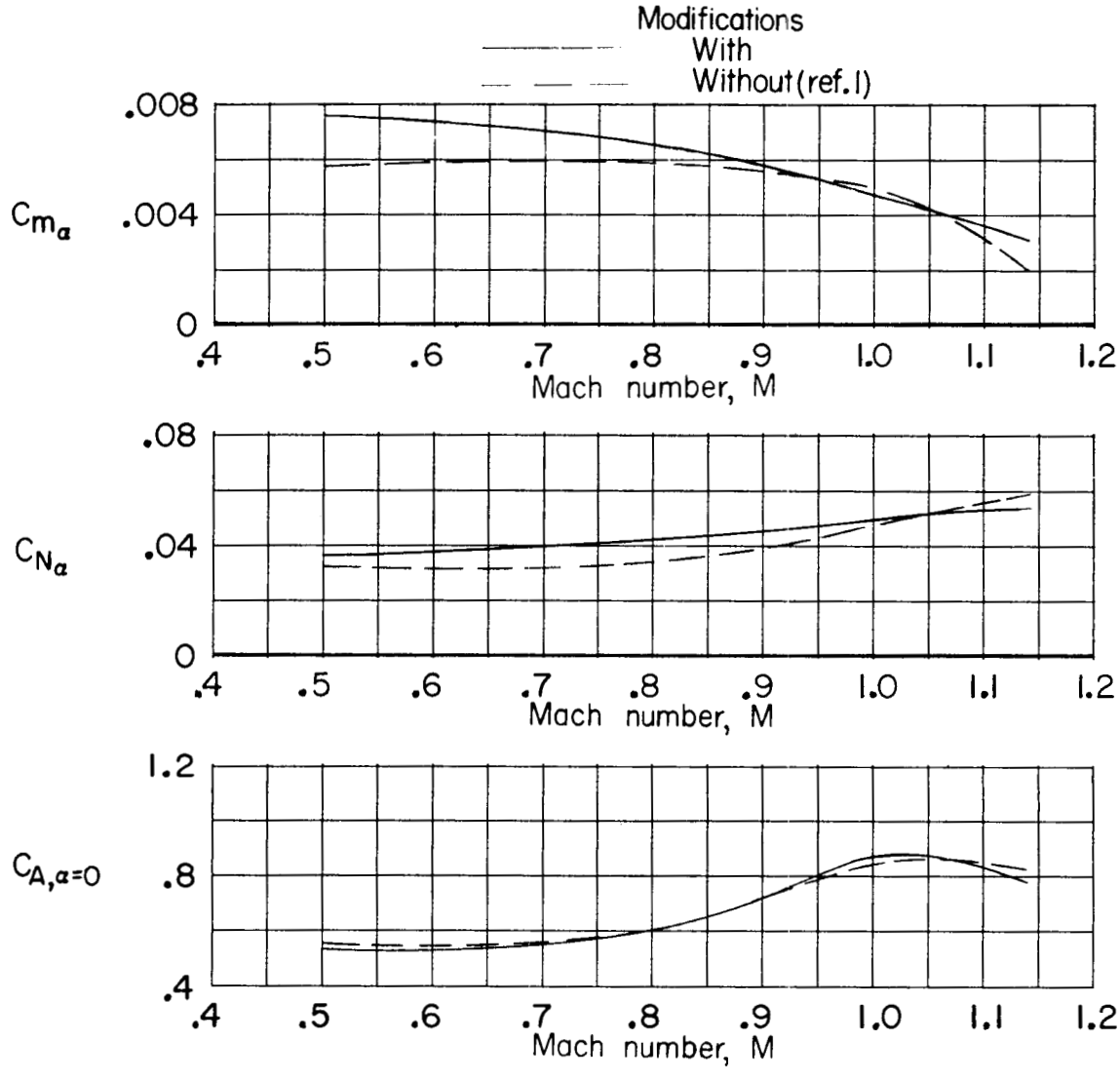

(d) Exit configuration with destabilizer flap and increased parachute-housing diameter.

Figure 9.- Concluded.

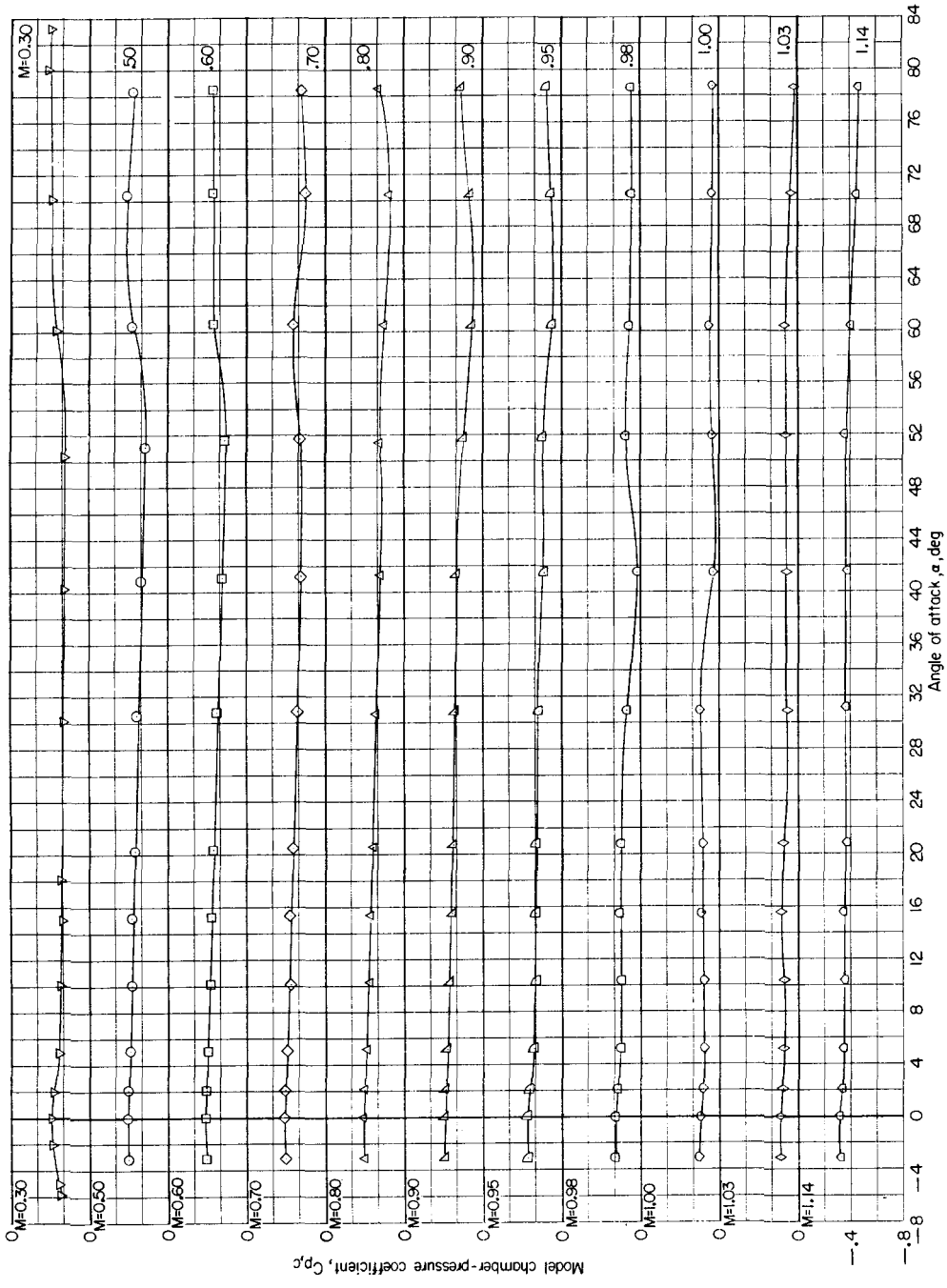

(a) Escape configuration.

Figure 10.- Variation of model chamber-pressure coefficient with angle of attack.

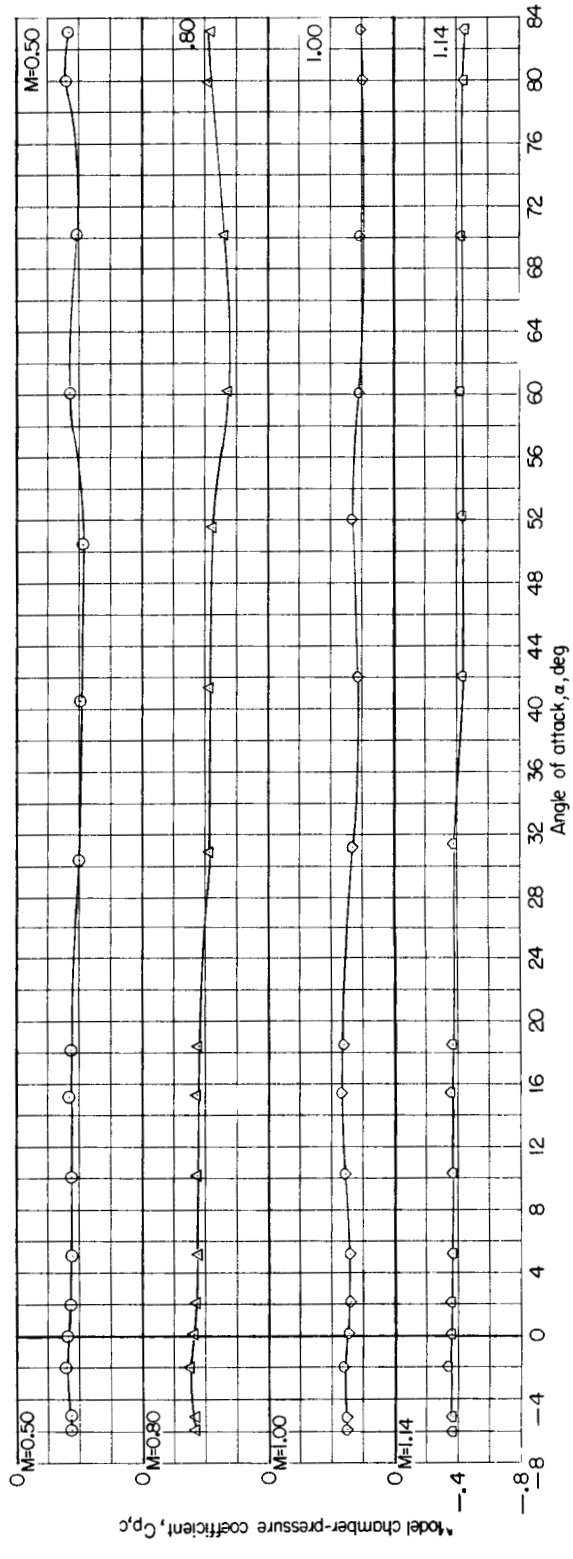

(b) Exit configuration.

Figure 10.- Concluded.